Out-of-Pile Experiments Performed in the U.S. Fuel Cladding Chemical Interaction (FCCI) Program by M.G. Adamson, the United States.

ABSTRACT

Since 1972 a variety of out-of-pile experiments have been performed as part of the U.S. National Fuel-Cladding Chemical Interaction (FCCI) Program. In the present paper results from these experiments are presented together with descriptions of many of the experimental techniques employed to obtain them. Although the main emphasis of the paper is on experiments designed to characterize FCCI with Type-316SS cladding, considerable attention is also paid to the following FCCI-related topics: thermodynamics of and phase equilibria in mixed oxide fuel and fission product compounds, fission product and cladding component thermo-transport, and chemical behavior of candidate oxygen-absorber materials (buffer/getters). Detailed interpretations of these results in terms of FCCI mechanisms are presented in a companion paper.

TABLE OF CONTENTS

I. INTRODUCTION

The purpose of this paper is to describe results from recent out-of-pile experiments that have been performed as part of the U.S. National FCCI program. Information of this type has previously been presented at IAEA meetings in Vienna in 1972 [1,2] and again in .1974 [3], so these dates will be used as a starting point for the work I will describe. Laboratory programs underway in the U.S. have the common objective of understanding the nature of fission product-induced cladding inner surface attack to a sufficient degree that approaches to eliminate the most pernicious form of this interaction - intergranular attack (IGA) - may be developed. More specific objectives of these programs may be stated as follows:

1. Characterization of the reaction behavior and thermomigration tendencies of the mobile and potentially aggressive fission products which accumulate in the fuel-cladding gap during fuel rod irradiations (i.e., Cs, I, Mo, Te.)

2. Identification of the specific fission products which cause localized deep intergranular penetrations of stainless steel cladding at characteristic oxygen activities $(p_{O_2})^{\dagger}$ for reference LMFBR Oxide fuel (initial O:M ratio = 1.97 ± 0.01).

3. Delineation of the critical parameters that control the IG attack rate and determine the mechanism of this chemical interaction.

---

†Oxygen activity $(p_{O_2}$, atm) and oxygen potential $(\Delta \bar{G}_{O_2} = RT\ell np_{O_2}$, kcal/mol) will be used interchangeably throughout the paper.

The first of these objectives requires a sound understanding of fuel rod chemistry and, to this end, a variety of thermodynamic measurements, phase studies and transport studies are also being performed as integral parts of the U.S. out-of-pile FCCI program. Particularly important here are oxygen potential -composition- temperature relationships for irradiated and unirradiated urania-plutonia fuel, thermodynamic stabilities and characterization of probable fission product reaction products, and oxygen, fission product and cladding component transport processes. Because of the strong consideration presently being given to introduction of chemical oxygen buffers and getters into oxide fuel rods (as FCCI inhibitors) out-of-pile chemical evaluations of the behavior of candidate buffer/getter materials are also in progress. Each of these FCCI-related topics will be covered in this presentation, however my main emphasis will be on experiments designed to characterize Type-316 stainless steel with respect to fuel-cladding chemical interaction. Detailed interpretations of these results in terms of FCCI mechanisms will be presented in a companion paper[4].

II. MEASUREMENTS AND TESTS DELINEATING THE EQUILIBRIUM THERMODYNAMICS AND THERMOTRANSPORT BEHAVIOR OF OXYGEN

A. Importance of Oxygen Thermodynamics

Irradiation of mixed-oxide fuel rods produces large radial temperature gradients and relatively small axial temperature gradients within the fuel. The magnitude of these temperature gradients is controlled by the thermal conductivity of the fuel, the rate of heat transfer across the fuel-cladding gap, the power level and the coolant temperature/flow rate. As an immediate consequence of the radial temperature gradient, four distinct structural regions generally develop in the fuel - a central void, a columnar grain region, an equiaxed grain region, and an unrestructured region. This restructuring is accompanied by the development of radial gradients in the oxygen potential and in the O:M and Pu:U+Pu ratios of the fuel. Since it is the oxygen potential at the outer surface of the fuel which provides the chemical force needed to drive the (oxidative) attack on the cladding material, it is important to understand transport and reaction processes which determine this parameter. Such processes include reactions involving fission products and oxygen redistribution. The oxygen potential gradient established across the fuel radius also determines the chemical states of reactive fission products, some of which are implicated in FCCI, and the ease of transport of a particular fission product to the cladding wall usually is a function of its chemical state.

B. Oxygen Potentials of Mixed Oxide Fuel

The chemistry that occurs inside a fuel pin during irradiation is necessarily complex, and a prerequisite to its understanding is reliable information about $O:M/Pu:U+Pu - \Delta \bar{G}_{O_2} - T$ relationships for mixed (U,Pu) oxide fuel inside an operating pin. Recent assessments of available oxygen potential data have revealed a number of discrepencies between "high" ($>1700^\circ C$) and "low" ($<1140^\circ C$) temperature $\Delta \bar{G}_{O_2}$ data for stoichiometric and slightly hypostoichiometric $U_{1-y}=Pu_z O_2$ ($z=0.1-0.3$). Indeed, there is considerable uncertainty about the oxygen potential value of exactly stoichiometric fuel at a typical reference temperature (e.g. at $850^\circ C$ $\Delta \bar{G}_{O_2} = -99 \pm 15$ kcal/mol).[5]

Woodley[6] recently repeated and extended some of his earlier vacuum-balance equilibrium measurements[7] on hypostoichiometric mixed oxide at low temperatures ($z=0.25$, $T= 900 - 1100^\circ C$). These results are illustrated in Figure 1, which shows good agreement between the two sets of data. A number of data points were obtained in the stoichiometry range $1.990 - 1.999$.

Tetenbaum[8] has also performed additional H_2O/H_2 gas mixture equilibrations with $U_{0.80}Pu_{0.20}O_{2-x}$ at 1027, 1065 and $1140^\circ C$. The resulting oxygen potential values are compared with Woodley's low temperature data (normalized to $z=0.20$) and predicted values from Blackburn's quasi-thermodynamic method[5] in Figure 2.

Also shown on this figure are Woodley, Markin and McIver,[9] and Tetenbaum's earlier data for hypostoichiometric mixed oxide. Tetenbaum's newest data are seen to fall between Woodley's measurements and Blackburn's calculations. In an attempt to resolve these discrepencies both workers recently made measurements on the same fuel specimen at 1300K (Pu:U+Pu = 0.20, O:M = 1.98). Again, Woodley's $\Delta \bar{G}_{O_2}$ value was 4-5 kcal/mol lower than Tetenbaum's value.
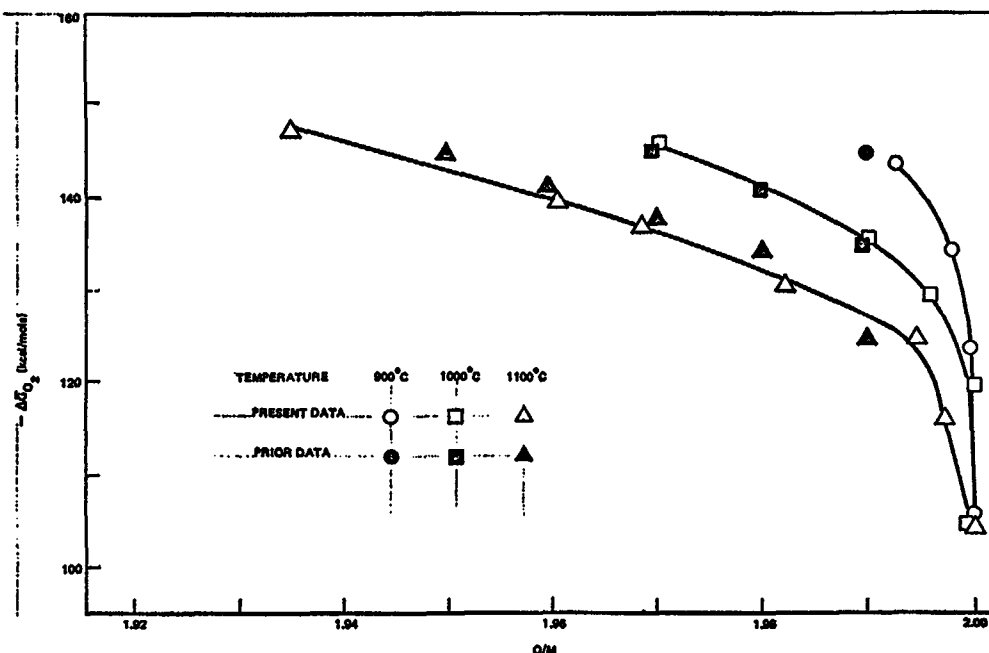
Figure 1 *Recent Oxygen Potential Data for Hypostoichiometric Mixed Oxide.*

In the course of making their measurements on mixed oxide fuel samples with slightly different Pu contents both Woodley and Tetenbaum have obtained data that cast doubt on the constant Pu valence approximation originally proposed for hypostoichiometric compostions by Markin and Rand. [10] In other words, in the composition range z = 0.10 to 0.30, approximately, the oxygen potential corresponding to a given Pu valence does not appear to be independent of Pu:U+Pu.

C. Oxygen Potentials of Fuel Plus Dissolved Fission Products

The oxygen potential of irradiated fuel with a particular O:M ratio depends upon its Pu:U+Pu ratio and the concentration of fission product elements that are dissolved in the oxide matrix. Although the variation in the oxygen potential of unirradiated fuel with O:M and temperature is known in some detail, equivalent data for fuel containing dissolved fission products have been very limited. Blackburn [5] has begun to modify his quasi-thermodynamic method for estimating oxygen potentials in unirradiated mixed oxide fuel to include dissolved fission products, however the output presently requires calibration against available data from systems such as U-Ce-O [8,11] and U-Nd-O [8]. Woodley [6], on the other hand, has recently applied his vacuum-balance equilibration technique to measure the oxygen potentials of
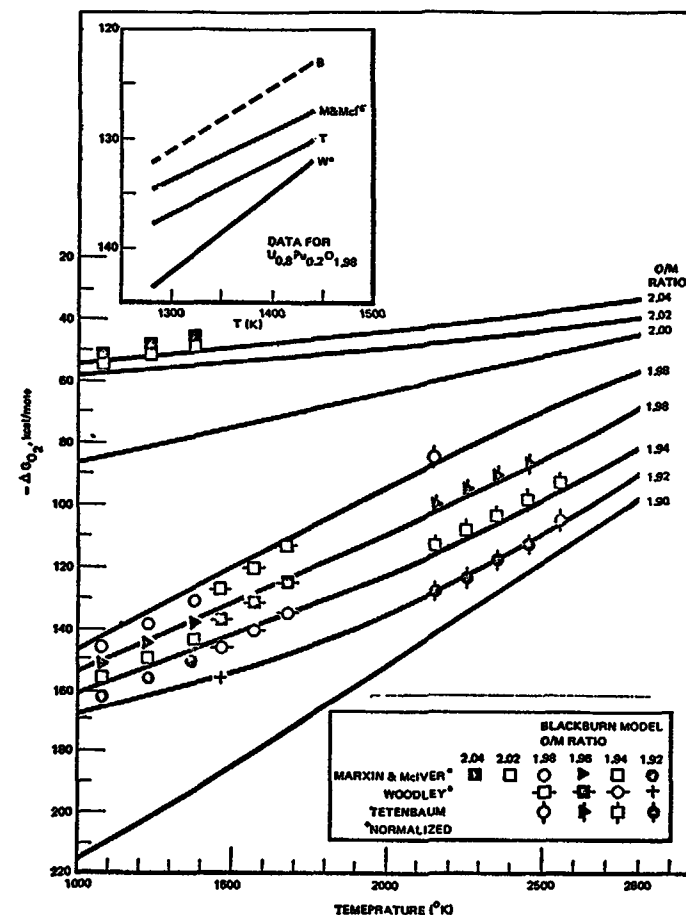
Figure 2 *Comparison of Measured Oxygen Potential to that Calculated with Thermodynamic Model for $U_{0.8}Pu_{0.2}O_{2 \pm x}$*

simulated irradiated fuels at 900°, 1000° and 1100°C. The compositions of the simulated fuels, which are shown in Table 1 , are based on burnups of 2, 5 and 10 atom percent. At each burnup six different fuel stoichiometries (O:M ratios)[†] were measured, the maximum deviation from stoichiometric composition being 0.05.

As anticipated from previous studies[8,11] at a given O:M and temperature, fuel containing dissolved fission products exhibits higher oxygen potentials than the undoped fuel, the increase ranging from 1 to 17 kcal/mol depending upon O:M and T. In general, the increase in $\Delta \overline{G}_{O_2}$ was found to be greater

---

[†]M = U + Pu + dissolved fission products; the absolute O:M ratio at "stoichiometric composition" varies from 1.997 (2 a/o) to 1.984 (10 a/o).

the lower the temperature and the smaller the deviation from "stoichiometry". Also, at a particular burnup and temperature, $\Delta\bar{G}_{O_2}$ was found to increase almost linearly with decreasing values of log x (where x is the deviation from "stoichiometry"). This trend facilitates interpolation or extrapolation to other fuel oxygen activity levels. The $\Delta\bar{G}_{O_2}$ variation with burnup at fuel temperatures of 900, 1000 and 1100°C was also found to be approximately linear up to 10 a/o burnup (see, for example, Figure 3). The enhancement of oxygen potential due to dissolved fission products (2.5 mol % Ce) is illustrated in Figure 4. This composition, $U_{.75}Pu_{.225}Ce_{.025}O_{2-x}$, corresponds to a burnup of ca. 3.5 atom %.

Table 1 . Composition of the Simulated Irradiated Fuels

Metal	Metal Mole Fraction			
	0 a/o B.U.	2 a/o B.U.	5 a/o B.U.	10 a/o B.U.
U	0.750	0.7538	0.7596	0.7696
Pu	0.250	0.2349	0.2117	0.1716
Pr	0	0.0009	0.0022	0.0046
Ce	0	0.0021	0.0054	0.0111
Zr*	0	0.0021	0.0052	0.0107
Nd**	0	0.0058	0.0148	0.0302
Y	0	0.0004	0.0010	0.0021

*Less amount reacted with Sr and Ba to form zirconates
**Includes contributions of La and Sm.

D. Thermodynamics of Fission Product Compounds.

Thermodynamic measurements have been made on a number of possible fission product compounds to evaluate their likelihood of forming inside irradiated mixed oxide fuel pins. A review paper, presented by O'Hare at the 1974 IAEA Thermodynamics of Nuclear Materials Symposium[12] , summarized the results of calorimetric measurements performed on a number of compounds, some of which may form inside intact LMFBR fuel pins (i.e. Cs_2MoO_4, $Cs_2Mo_2O_7$, Rb_2MoO_4, $BaMoO_4$, Cs_2O, Cs_2UO_4, $Cs_2U_2O_7$, Rb_2UO_4 and Cs_2CrO_4). Standard enthalpies of formation at 298.15K, $\Delta H°_f(298.15)$, were measured for all of these compounds, and in some cases sufficient heat capacity $(C_p°)$ and enthalpy increment $(H°(T)-H°(T_{ref}))$ data were obtained to give entropies $S°(298.15)$, and hence the
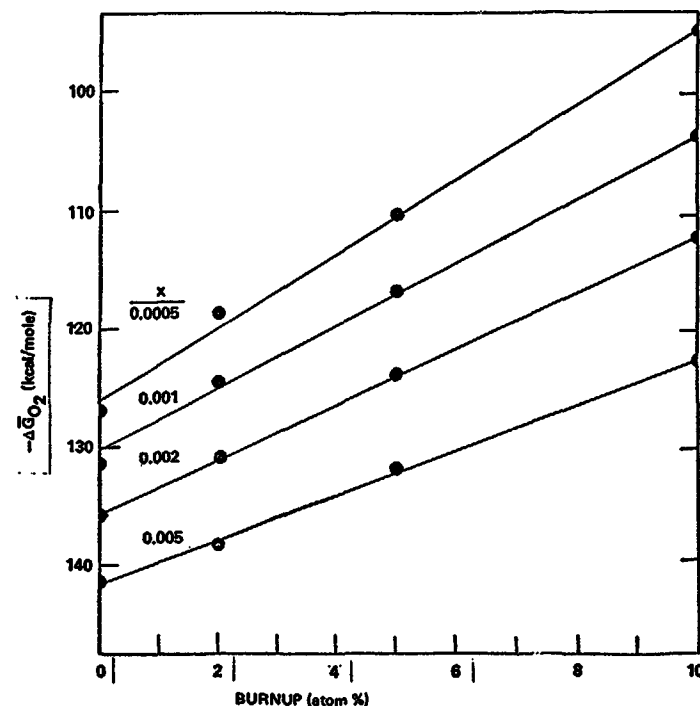
FIGURE 3. VARIATION OF $\Delta\bar{G}_{O_2}$ WITH BURNUP FOR SIMULATED IRRADIATED FUEL

DATA POINTS FOR Ce-DOPED FUEL.
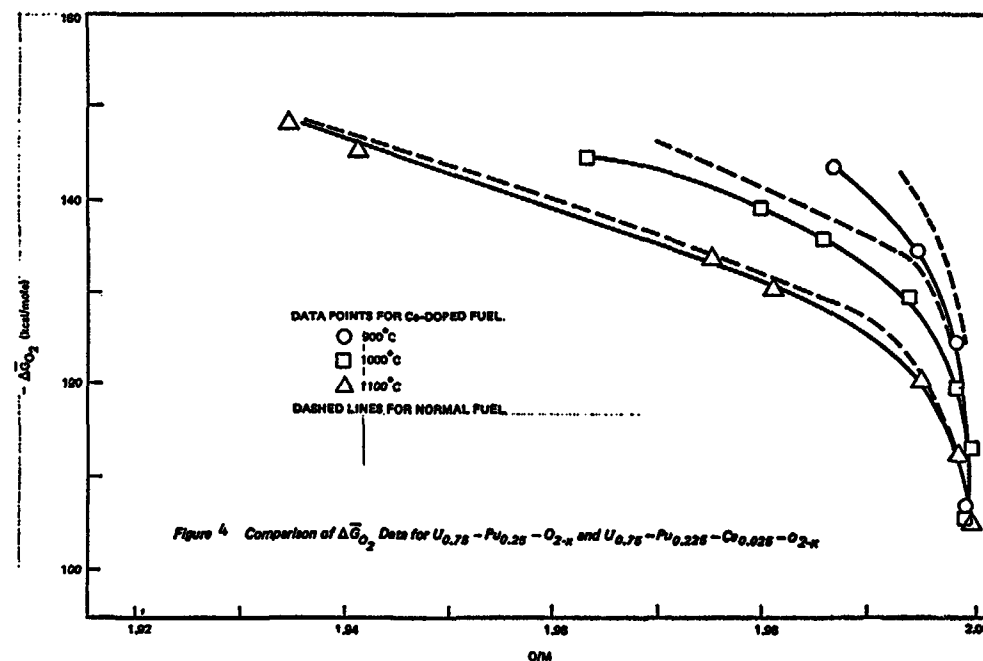O 900°c
□ 1000°c
△ 1100°c

DASHED LINES FOR NORMAL FUEL.

Figure 4   Comparison of $\Delta\bar{G}_{O_2}$ Data for $U_{0.75}-Pu_{0.25}-O_{2-x}$ and $U_{0.75}-Pu_{0.225}-Ce_{0.025}-O_{2-x}$

standard Gibbs energy of formation, $\Delta G°_f$, as a function of temperature. More recent calorimetric measurements at ANL have filled in gaps in the data for the compounds listed above and provided new data for compounds such as $Cs_2Cr_2O_7$, Cs_3CrO_4, CsOH, $BaUO_4$ and $CaUO_4$[13]. A mass spectrometric study of the vaporization of cesium molybdate has also been made[14], and from this an equation was derived for the temperature-dependence of the pressure of $Cs_2MoO_4(v)$ over Cs_2MoO_4 (c and ℓ). In this study the Gibbs energy of formation of $Cs_2MoO_4(v)$ was also obtained over a limited range of temperature (1070 -1170 K). A high temperature galvanic cell technique, employing an yttria-doped thoria solid oxide electrolyte, has been employed to measure equilibrium oxygen activities in systems such as $Cs_2UO_4(c)/UO_2(c)/Cs(\ell)$, $O(dissolved)/Cs(\ell)$ and "Cs_xNbO_y"/ NbO(c)/Cs(ℓ).[14] From these type of EMF cell data, some of which are summarized in Figure 5, it is possible to make direct comparisons of reaction product stabilities (either as equilibrium oxygen potential values or via $\Delta G°_f$ - T data).
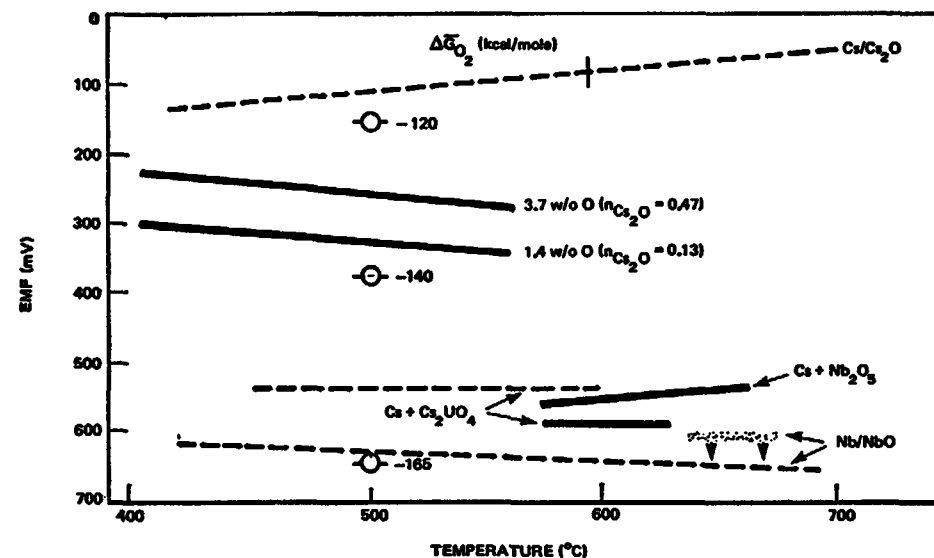
Several of the thermodynamic measurements mentioned above have been performed as adjuncts to phase characterization studies. Clearly a reliable evaluation of fission product compound formation inside irradiated fuel pins cannot be made unless all possible phases that could form in the multi-component fuel pin system are known. Although the available thermodynamic data suggest that the only Cs-fuel compounds capable of forming inside irradiated fuel pins are Cs_2UO_4 and possibly $Cs_2U_2O_7$ (i.e. compounds of VI-valent uranium), some evidence has been obtained that lower-valent Cs-U,Pu-O compounds analogous to those formed in the Na-U,Pu-O system, form when Cs fission products react with mixed oxide fuel at low oxygen activity.[3,15]Some attempts have been made to characterize these lower-valent compounds (Cs_xMO_y),[3] including an assessment of the stabilities of normal- and poly-uranates of cesium [16], however questions concerning their composition and existence inside irradiated fuel pins are still unresolved. Further discussion of the most likely chemical states of the "reactive" fission products Cs,Rb,Te,Sr,I,Br and Mo inside irradiated mixed oxide fuel pins will be found in a companion paper[4].

E. Oxygen Redistribution in Temperature Gradients

Two computational models for calculating radial oxygen distributions in irradiated fuel pins have been developed in the United States, one at GE, the other at ANL. The GE model[17] involves the operation of alternative thermotransport paths for oxygen atom migration, namely, ionic diffusion in

Figure 5 EMF Cell Results for Cs—Oxide Equilibria (In/In$_2$O$_3$ Reference Electrode)

the solid and gas phase transport via H_2/H_2O or CO/CO_2, which lead to a cyclical flow of material. Their non-equilibrium model employs heats of transport derived from laboratory thermal gradient experiments on mixed oxide fuel[17]. It is assumed that isothermal surfaces in the fuel eventually achieved constant stoichiometric(0:M ratio), so axial 0:M profiles may also be generated. Although the model allows oxygen to move axially, oxygen is conserved in the fuel column.

The ANL model[18] assumes that oxygen movement is controlled by ionic diffusion, the driving force being the product of an activity-independent diffusion coefficient and the oxygen activity. A steady-state oxygen distribution is achieved when no gradient exists within the fuel in terms of the product of the appropriate diffusion coefficient and the oxygen activity. Lattice diffusion is assumed to depend on oxygen activity for low 0/M fuel and to be limited by low vacancy concentration in near-stoichiometric fuel. In its present form this model only calculates radial oxygen distributions.

Both models were recently tested by applying them to a radial section of an EBR-II test pin (HEDL-P-23A-31). The initial 0:M of the fuel in this pin was 1.984 (25 w/o PuO_2) and the time-averaged peak pin power was 11.9 kW/ft. The calculated radial temperature profile at the section of interest (13.4 inches above the bottom of the fuel column) is shown below.

r (in) (cm)	r/r₀	Temp.(°C)	(°F)
0.010 (0.025)	0.10	2097	3807
0.019 (.048)	0.20	2097	3806
0.029 (.074)	0.30	2072	3761
0.039 (.099)	0.40	2019	3667
0.049 (.124)	0.50	1941	3525
0.058 (.147)	0.60	1838	3340
0.068 (.173)	0.70	1713	3115
0.078 (.198)	0.80	1542	2808
0.088 (1.224)	0.90	1352	2465
0.097 (.246)	1.00	1148	2099

Results for the beginning-of-life radial O:U+Pu profiles are presented in Figure 6. Both models yield the same qualitative results for the test case conditions, i.e. redistribution of oxygen down the thermal gradient to the
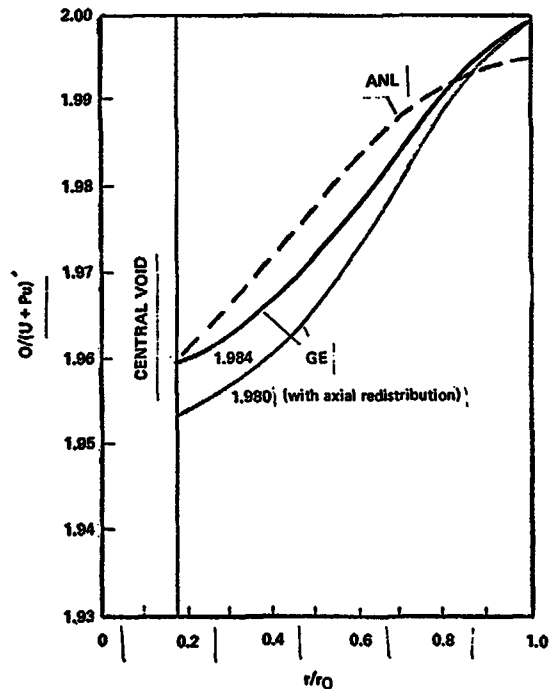

FIGURE 6. PREDICTED BEGINNING-OF-LIFE RADIAL OXYGEN-TO-METAL
(O/U+Pu) PROFILES FOR P-23A TEST CASE (AVERAGE O:M = 1.984)

periphery of the fuel; however, differences in the quantitative results from the two models are significant. As illustrated in the figure, the two models predict different radial oxygen profiles. The GE model predicts the greater oxygen redistribution, resulting in a higher O/M at the fuel surface and, consequently, a more oxidizing environment to the cladding. Currently, experimental data from in-reactor tests are not available for evaluation and selection of one model over the other based on quantitative comparisons. An important difference between the two models that should be noted is that the GE model predicts oxygen migration up a thermal gradient to the fuel center for a hyper-stoichiometric fuel, in qualitative agreement with observed in-reactor behavior.[19] The ANL model, on the other hand, predicts only migration down a thermal gradient regardless of the fuel stoichiometry.

III. TESTS TO CHARACTERIZE CHEMICAL ATTACK OF TYPE 316SS CLADDING

A. Experimental Methods and Earlier Findings; Identification of Aggressive Fission Products

Isothermal anneal capsules and thermal gradient capsules have been used in out-of-pile experiments at different laboratories. These experiments consisted of encapsulating various fission products or mixtures of fission products in ratios that roughly approximated the fission-product yields. Generally, a controlled oxygen potential was maintained within the capsule by using $(U,Pu)O_2$ or a buffer mixture. Buffer materials in order of increasing oxygen activity included Cr/Cr_2O_3, Cr_3C_2/Cr_2O_3, Fe/FeO, Ni/NiO, and Cu/Cu_2O. The capsules were heated isothermally or placed in a temperature gradient for various lengths of time. The isothermal anneal experiments served to identify the fission products and establish the conditions required to cause intergranular attack. The thermal gradient experiments were performed to determine both the migration characteristics of volatile fission products and the interactions of fission products at controlled oxygen potentials. Some of the initial isothermal capsule tests[1,2] established that $Cs_2O,CsOH$ and tellurium are very aggressive in promoting intergranular attack of 300-series austenitic stainless steels at 650°C; however, it was recognized that these particular chemical forms of Cs and Te fission products may not be the forms that exist at the interface inside a mixed oxide fuel pin.

Results from the early thermal gradient experiments performed at General Electric (GE) indicated that tellurium (in combination with cesium) has a unique role as a cladding attack initiator since it was found to be an essen-

tial ingredient for inducing severe intergranular attack in cladding samples at oxygen potentails between the oxidation threshold for stainless steel (~-135 kcal/mol at 725°C) and slightly hyperstoichiometric fuel (~-80 kcal/mol). Intergranular penetration of cladding samples inside the thermal gradient capsules was observed at 850°C and lower* for Cs:Te ratios ≤ 2. The apparent dependence of attack incidence on Cs:Te ratio suggested that a mass action effect on Te activity was operative; i.e. , Te only influenced oxidative attack when its activity exceeded a certain value. In addition, the dependece of the Te-catalyzed oxidative attack process on both Te activity and oxygen potential showed a strong resemblance to essential features of sulfur-catalyzed hot corrosion of the super alloys used in gas turbine blades.[20] In this latter process, small quantities of sulfur impurity that are deposited (as sulfate) on alloy surfaces during combustion can initiate severe oxidative attack when the oxygen potential at the alloy surface becomes sufficiently low to release sulfur from the sulfate. By forming nickel and chromium sulfides in the alloy matrix, this sulfur effectively sensitizes the alloy to oxidative attack (the sulfides being more susceptible to oxidation), and the sulfur is believed to behave as an autocatalyst.[20] Since Te and S belong to the same peridoic group of elements (VI) and exhibit similar reaction trends with the transition metals that constitute austenitic alloys, it was logical to suspect tellurium fission products as possible cladding attack initiators in the LMFBR fuel rod system. Indeed, intergranular cracking developed in Hastelloy N and related alloys during exposure to irradiated molten salt fuels has been attributed to reaction with tellurium fission products. [21] The thermomigration experiments performed with Cs and Te also showed that some Cs can migrate preferentially down a temperature gradient if the overall Cs:Te ratio of the fission product mixtures exceeds ~2. Hence, even if all the Cs and Te fission products are originally deposited in the fuel-cladding gap of an irradiated fuel rod in amounts corresponding to their overall fission yield ratio (5:1 to 7:1), it seems clear that subsequent preferential (axial) migration of Cs along the fuel column will produce Cs,Te deposits at certain localities with Cs:Te ratios favorable for cladding attack.

---

* The lowest temperature at which attack was observed was 750°C, but the lower temperature limit for intergranular attack could not be determined in this type of experiment because the test duration (100 hours) limited the distance Cs,Te moved down the thermal gradient.

The initial emphasis of the General Electric isothermal capsule test program was to achieve a better definition of the conditions under which deep intergranular penetration of Type-316 SS cladding occurs at 725°C. In this phase of the investigation, the principal variables were oxygen potential ($\Delta \bar{G}_{O_2}^{725°C}$ =-140 to -46 kcal/mol O_2), Cs:Te ratio (0:1 to 8:1) and the effects of added impurities such as carbon and the fission products iodine (as CsI) and molybdenum (as Mo, MoO_2 and Cs_2MoO_4). Later work focused on kinetic and mechanistic aspects of the Cs,Te-induced cladding oxidation, time (0-1000h) and temperature (450-1000°C) being varied systematically at two representative oxygen activity levels: "high" (Fe/FeO buffer) and "low" (Cr_xC/Cr_2O_3 buffer).

To simplify results from these isothermal capsule experiments the amounts of Cs and Te fission products used was considerably in excess of the Cs and Te concentrations expected on the cladding inner surface in irradiated fuel pins. More recently, the dependence of intergranular attack rate on Cs + Te inventory, and the effect of the surface condition of Type-316SS cladding specimens have been investigated. The mechanism of carbon participation in the Cs,Te-induced cladding attack process at "low" oxygen activities (i.e., conditions which lead to deep intergranular penetration) has also been investigated using a combination of radiotracer (C-14) and electron microbeam (SEM-EDAX) techniques. Although the majority of the isothermal capsule experiments were performed with capsules fabricated from lengths of tubing of the cladding under study, some of the more recent tests performed at GE utilized Type-316SS specimens in the form of rectangular coupons (1X1X13 mm). These coupons were imbedded in fission product buffer mixtures at the bottom of small nickel capsules. An alternative test design has recently been employed at Hanford Engineering Development Laboratory (HEDL) to study the effects of common fabrication impurities on the Cs, Te-induced attack of Type-316SS. In this design, mixtures of Cs, Te and various impurities are squeezed between a mixed oxide fuel pellet and a section of cladding during the high temperature treatment. Schematics of these various test designs are illustrated in Figure 7

B. Delineation of Conditions for FCCI

Earlier isothermal capsule experiments demonstrated that, under otherwise optimal conditions for fission product-induced cladding attack ($1:1 \leq Cs:Te \leq 3:1$, T ~ 725°C, presence of carbon), the character of the attack process changes from "deep intergranular" to a shallow combination of intergranular and matrix reaction as the oxygen activity level increases from 4.6×10^{-30}-ca 5.6×10^{-29} atms ("low" regime) to ca. 5.6×10^{-29}-ca. 3×10^{-18} atms("high" regime). The

commences at $\sim$550°C. Between 650 and 725°C the rate becomes "rapid" and the depth of intergranular penetration increases progressively with temperature; at 900°C the separation between the intergranular penetration front and the general reaction front was 10 mils. At "low" oxygen activities deep intergranular penetration was found to occur when $1:1 \leq Cs:Te \leq 3.1$, but between 3:1 and 4:1 the character of attack of Type-316 stainless steel was noted to change from "intergranular" to a shallower, more uniform matrix reaction.

Oxygen Activity Effects. Several isothermal capsule experiments were recently performed[22] to obtain additional information about the Cs,Te-induced intergranular penetration of Type-316SS that occurs in the vicinity of and somewhat above its lower oxygen activity threshold. The experiments were performed both in the presence and absence of added carbon using as buffer mixtures coexisting pairs of phases from the Nb-O and V-O systems (Nb/NbO, NbO/NbO_2, NbO_2/Nb_2O_5, -and VO/V_2O_3). Conditions, capsule contents and results for this series of tests are summarized in Table2 :

(a) TYPE-316 STAINLESS STEEL TEST CAPSULE (GE)

(b) NICKEL CAPSULE CONTAINING COUPON SPECIMEN (GE)

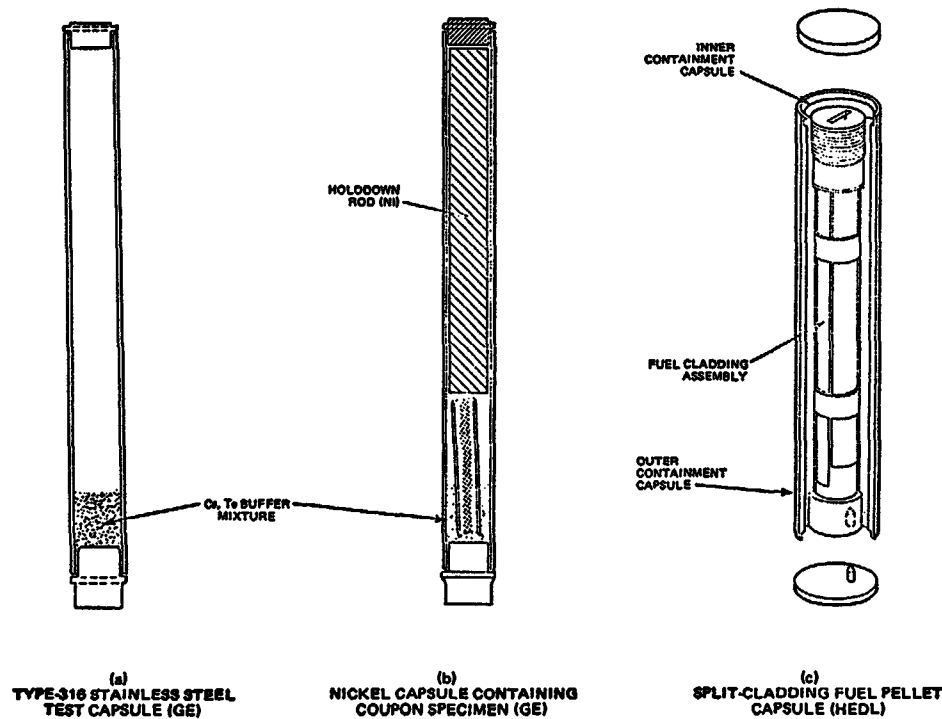(c) SPLIT-CLADDING FUEL PELLET CAPSULE (HEDL)

Figure 7 Schematic of Isothermal Capsule Test Designs

lower and upper bounds of these two oxygen activity regimes correspond to mixed oxide fuel compositions of $U_{0.75}Pu_{0.25}O_{1.996}$ and $U_{0.75}Pu_{0.25}O_{2.000}$ (approximately). At even higher oxygen activities, $po_2 > 3.8 \times 10^{-17}$ atms, deep intergranular penetration of stainless steel cladding can be caused by cesium alone (Cs_2O and higher oxides), however, such high oxygen activities, which correspond to hyperstoichiometric fuel, are not expected to develop in reference-design LMFBR oxide fuel pins. The effect of temperature on the character of Cs,Te-induced oxidation of Type-316SS was also delineated at "high" and "low" oxygen activities by a series of isothermal capsule tests. At "high" oxygen activities oxidation commenced at $\sim$500°C, forming a thin coherent oxide film which thickens up to temperatures $\sim$650°C. Above 650°C oxidation of the cladding takes the form of general matrix reaction in which intergranular attack never precedes the uniform reaction front by more than 1.5 mils. At "high" oxygen potential the attack rate does not become rapid ($d_{max}^{100} > 2$ mils) until T>800°C. At "low" oxygen activities initial oxidative attack is intergranular and

CONDITIONS AND CAPSULE CONTENTS FOR TYPE-316 STAINLESS STEEL FISSION PRODUCT ATTACK TESTS WITH Nb-O AND V-O BUFFER MIXTURES

Test Conditions: 725°C/100h
Specimens: annealed 316 stainless steel tubing

Capsule No.	Quantities of Additives (millimoles)			Results/Observations
	Cs	Te	Other	
36-1	0.39	0.39	Nb=NbO=0.25	No Attack
36-2			NbO=NbO_2=0.25	No Attack
36-3			NbO_2=NbO_2.5=0.25	Intergranular Attack, d_{max} = 4.4 mils (112 μm)
36-4			NbO_2=NbO_2.5=0.25 C=0.6	Intergranular Attack, d_{max} = 4.7 mils (119 μm)
36-5			VO=VO_1.5=0.25	Deep Intergranular Attack, d_{max} = 5.7 mils (145 μm)
36-6	0.39	0.39	VO=VO_1.5=0.25 C=0.6	Deep Intergranular Attack, d_{max} = 8.6 mils (218 μm)

Table 3
EQUILIBRIUM OXYGEN POTENTIAL/OXYGEN ACTIVITY VALUES FOR
SELECTED BUFFER MIXTURES AT 725°C AND EFFECT ON TYPE-316
STAINLESS STEEL COMPATIBILITY WITH Cs,Te MIXTURES (Cs:Te=1:1)

Buffer Mixture	ΔG_{O_2} (kJ/mol)*	p_{O_2} (atm)	Compatibility
'Nb'/NbO	-654	5.95×10^{-35}	No Attack
NbO/NbO$_2$	-587	2.00×10^{-31}	No Attack
Cr/Cr$_2$O$_3$	-585	2.56×10^{-31}	No Attack
Type-316SS Oxidation	-565±8	2.75×10^{-30}	
'VO'/V$_2$O$_3$	-564	2.90×10^{-30}	Deep Intergranular Attack; 6 mils (152 μm)
Cr$_3$C$_2$/Cr$_2$O$_3$(/C)	-540	5.74×10^{-29}	Deep Intergranular Attack; 5 mils (127 μm)
NbO$_2$/Nb$_2$O$_5$	-481	5.38×10^{-26}	Intergranular Attack; ~4 mils (102 μm)

*The oxygen potential is defined as $\Delta G_{O_2} = RT \ln p_{O_2}$ /atm); free energy changes are expressed in the units
kilojoules (1kJ=0.239kcal) per mole.

The oxygen potentials established by these "new" buffer mixtures at 725°C
are listed in Table 3 , together with calculated potentials for the stainless
steel oxidation threshold, and various chromium-chromium oxide-chromium
carbide mixtures. In deriving these oxygen potentials it is tacitly assumed
that reaction between cesium and one (or both) of the metal oxides, which
could alter the equilibrium $\overline{\Delta G}_{O_2}$ value, is not significant. Previous tests
have shown this assumption to be valid, especially when the Cs:Te ratio is
low (i.e., Cs reacts preferentially with Te when Cs:Te<2:1).

The results show that no intergranular attack occurred at the oxygen activities
established by Nb/NbO and NbO/NbO$_2$, but severe attack occurred with VO/V$_2$O$_3$.
According to the oxygen activities listed in Table 3 , NbO/NbO$_2$ lies just below
the oxidation threshold for Type-316 stainless steel while VO/V$_2$O$_3$ (and Cr$_2$O$_3$/
Cr$_3$C$_2$) lie just above this threshold potential. The agreement between the
experimentally determined threshold for Cs,Te-induced intergranular attack
of Type-316 stainless steel (-585 kJ/mol<$\Delta \overline{G}_{O_2}$725°C<-564 kJ/mol) and the esti-
mated/measured threshold for uncatalysed (gaseous) oxidation of the same alloy
($\Delta \overline{G}_{O_2}$725°C = 565 ± 8 kJ/mol) is so close that the two thresholds are believed
to be coincident.

Intergranular attack also occurred with the NbO$_2$/Nb$_2$O$_5$ buffer, which establishes
an oxygen potential ca.60 kJ/mol higher than the upper oxygen activity limit
for stability of grain boundary carbide phases in the cladding -540 kJ/mol
at 725°C). The maximum intergranular penetration depth under these conditions
was 4.4 mils (112μm), which is significantly less than the penetration obtained
within the oxygen activity range of carbide stability, i.e., 5.7 mils/145μm
(VO/V$_2$O$_3$ buffer). Although the attack depth obtained with NbO$_2$/NbO$_{2.5}$ is

considerably more than the previously determined attack depth with Fe/FeO
(1.5 mils/38μm)[3], certain features of the intergranular penetration obtained
with this buffer suggest that it could be classified as a "high" oxygen acti-
vity regime buffer (see following section entitled "Carbon Impurity Effects").

CAPSULE 36-4   AS POLISHED   250X

CAPSULE 36-5   AS-POLISHED   250X
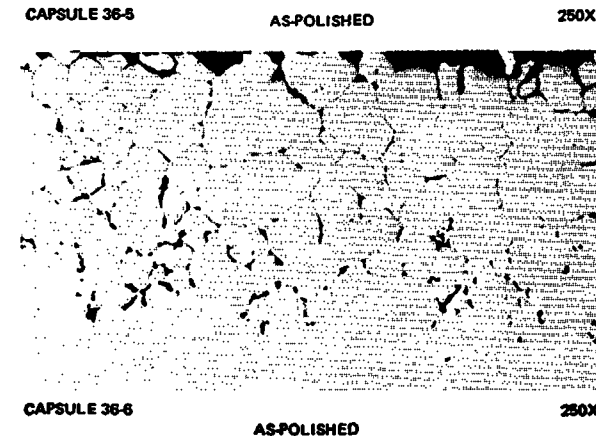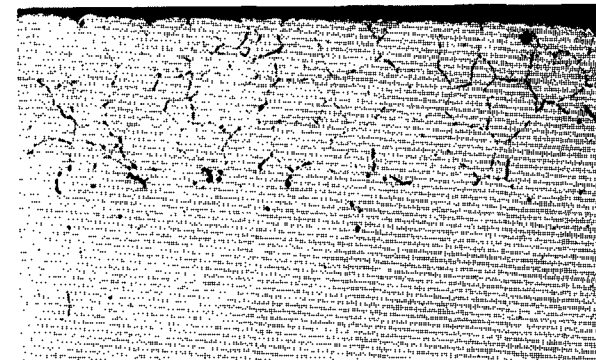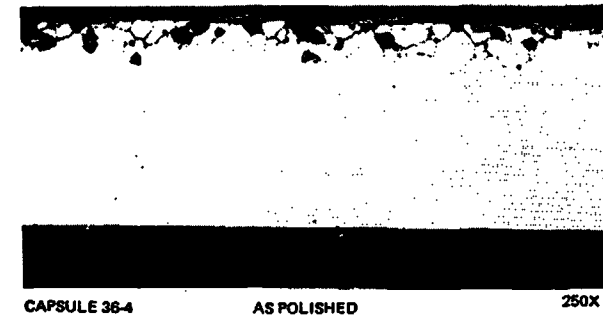

CAPSULE 36-6   250X
AS-POLISHED

*Figure 8   Photomicrographs of Attacked Inner Surfaces of Type-316 Stainless Steel
Capsules Exposed to Cs, Te-NbO$_2$, Nb$_2$O$_5$ (C) (36-4) and Cs, Te-VO,
V$_2$O$_3$ (C) (36-5 and 36-6) Mixtures (Cs: Te=1:1, 100h at 725°C)*

The photomicrographs shown in Figure 8 illustrate the results obtained with NbO_2/NbO_5 and VO/V_2O_3 buffers. The areas photographed are representative of positions of maximum intergranular penetration on the inner walls of each capsule.

C. Rate Measurements

Out-of-pile experiments to determine the rate of intergranular penetration of Type-316SS by Cs,Te fission product mixtures have been performed at Argonne National Laboratory (ANL) and at GE.[23,24] In each of these studies the quantities of Cs and Te used represented an excess compared to quantities expected to reach the cladding in an irradiated fuel pin. This was done to avoid the possibility that the maximum depth of penetration would be limited by the fission product inventories. In Maiya and Busch's work[23] 20% cold-worked 316SS cylinders were exposed to 2:1 Cs:Te mixtures at temperatures between 550-700°C in long temperature gradient capsules. Although an attempt was made to buffer the Cs,Te mixture in these tests, the capsule geometries prevented the establishment of known oxygen activities. Parabolic reaction kinetics were observed at 550-700°C, however, preliminary results for higher temperatures (>760°C) indicated the onset of slower penetration kinetics (i.e., time exponent n < ½). This type of fall-off in penetration kinetics with increasing temperature is recognized to be consistent with the Fisher-Whipple model for grain boundary diffusion from a free external surface.[23] At GE,time-dependent isothermal capsule tests were performed at 650, 725 and 800°C at "high" (Fe/FeO/C) and "low"(Cr/Cr_2O_3/C and VO/V_2O_3) oxygen activities. In each series of tests separate capsules were run for six different times. After heat treatment, each capsule was sectioned longitudinally, polished, and the maximum depth of attack determined. Considerable variations in attack depth occurred in the longitudinal sections, particularly in samples from the tests performed at 800°C. The scatter in the 800°C data was too great to warrant plotting them on a log-log graph (i.e., to obtain the time exponent in the rate law). However, the 650°C result showed considerably less scatter, and indicated approximately linear kinetics at "low" oxygen activity (n = 0.85 + .1 and parabolic kinetics at "high" oxygen activity (n = 0.55 + .15). Results at 725°C (VO/V_2O_3 buffer) - see Table 4 -showed minimal scatter and indicated a transition from nearly linear kinetics at short times to $t^{\frac{1}{4}}$ kinetics at longer times (>10 hours).

TABLE 4

Time-Dependence of Intergranular Penetration into 316SS by Cs,Te at 725°C

Cs:Te = 1:1   Buffer = VO/V_2O_3

Time(hrs)	Maximum Depth of Attack (Mils)
3.5	1.9+.4
10	3.9+.5
35	5.2+.2
100	5.7+.6
315	7.3+.4
1000	7.9+.3

The static character of the GE time-dependent capsule tests, and consequent inhomogeneities in reactant distribution on the cladding inner surface, is believed to be the factor primarily responsible for the observed variability of attack depth with position. Similar inhomogeneities are likely to occur on the cladding inner surface in irradiated fuel rods, and these inhomogeneities may lead to the observed variability of cladding attack.

D. Effects Related to Cladding Surface Condition

The effects to be described in this section-surface precarburization, scratches and indentations, and cold working-can equally well be regarded as secondary carbon effects, since, under conditions designed to produce Cs,Te-induced intergranular attack, the resulting alloy corrosion behavior appears to be influenced by the degree of carburization and/or the carbide particle morphology in the region of interest.

Surface Pre-carburization. Attempts to pre-carburize the inner surfaces of annealed Type 316H stainless steel capsules were made by immersing open capsules containing ~1 gram quantities of either Fe_3C or Cr_3C_2 in liquid sodium for 150 hours at 900°C.[22] Following the 900°C heat treatment, but before opening the outer nickel container, the temperature was reduced to 650°C for 100h (to precipitate carbide phases in the stainless steel grain boundaries). One capsule representative of each type of carburization conditions was sectioned and examined metallographically to determine the extent and distribution of carburization. From these it was readily apparent that although severe carburization occurred, its distribution was not uniform on the stainless

steel surfaces. Extensive inter- and intragranular carbide precipitation was also noted across the thickness of the capsule wall. Two Type-316H stainless steel capsules that had been treated identically to the carburization "controls" were loaded with a Cs,Te ($Cs:Te=1:1$)+Cr/Cr_2O_3C buffer mixture and heat treated at 725°C for 50 hours. Although the locations of heavy carburization in these two capsules could not be predicted, it was reasoned that at least a fraction of the stainless steel surface in contact with the fission product mixture would be "heavily carburized" and, therefore, distinguishable by its (different) attack morphology. This expectation was based, in part, on the supposition that heavily carburized regions of Type-316 stainless steel alloy would contain significant quantities of M_7C_3- and M_3C_2-type carbides which, on the basis of previous work at GE, are believed to be particularly susceptible to Cs,Te-assisted oxidation. The Type-316 stainless steel capsule that had previously been heat-treated with Fe_3C in sodium showed two rather distinct types of "uniform" attack on the inner surface. Near to the bottom of the capsule the reaction layer was thin ($\sim$1 mil/2μm) and apparently coherent; 1/2 to 3/4 inch above the bottom end plug a transition to a deeper, less coherent reaction layer occurred. Approximately 3 mils (76μm) of cladding was consumed by reaction in the upper part of the capsule and, although the leading edge of the reaction front clearly followed alloy crystal boundaries, intergranular penetration into the sound alloy did not occur. The capsule that was carburized with Cr_3C_2 in sodium showed essentially the same type of reaction as the upper part of the previous specimen (i.e., general consumption of surface grains) but also differed in two important respects: (a) the reaction depth varied from position to position (1 to 4 mils/25 to 102 μm) and (b) some intergranular penetration did occur in nonconsumed parts of the alloy matrix. It was concluded from these results that the general effect of heavily pre-carburizing Type-316 stainless steel cladding is to increase its susceptibility to uniform/matrix attack relative to intergranular attack. Initially, this result was surprising, since the original intention of the precarburization treatment was to nucleate higher carbide phases in the cladding grain boundaries -thereby increasing their susceptibility to attack. However, if the surfaces of the pre-carburized specimens are rich in higher carbide phases (as indicated by metallographic results), the expected form of attack by Cs,Te mixtures at low oxygen activity would appear to be uniform rather than intergranular.

Cold Work. Cold-working of austenitic Type-316 stainless steel produces transgranular deformation interfaces (slip lines) along which $M_{23}C_6$-type carbides can precipitate during subsequent heat treatment. These intragranular carbide precipitates may be expected to reduce the effective grain size of the alloy

by offering an increased reaction area for the fission product attack mixture. As noted later, (section IV-G), the maximum intergranular penetration depth of 300-series austenitic stainless steels by fission products at a given time and temperature is proportional to the average grain size of the alloy; on this basis, one would expect heavy cold working near the alloy surface to reduce the maximum intergranular penetration depth.

Some evidence that cold-work on the surface of an alloy sample can "absorb" fission product corrodants has been obtained from buffered Cs,Te attack tests performed at GE on a variety of alloy coupon specimens with polished and unpolished (as-cut) surfaces.[25] One such Type-316 stainless steel specimen that was exposed to a 1:1 Cs,Te mixture (Cr,Cr_2O_3,C buffer) for 100h at 725°C exhibited a maximum intergranular penetration depth approximately 25% greater on the polished side than on the as-cut side (which contained residual cold work). With smaller grained specimens, and specimens only attacked to a depth of 5 mils or less, differences in the observed attack depth between polished and unpolished surfaces were scarcely detectable. Similar results were obtained from fission product attack tests performed on annealed and 20% cold worked "reference" cladding materials at "high" oxygen activity (Fe/FeO buffer). It is inferred from these results that the primary factor determining whether or not cold work inhibits fission product-induced intergranular attack is the degree of cold work in the surface of the cladding alloy. Further tests are required to elucidate this point.

Scratches and Indentations. The potential for scratches on the surface of Type-316 stainless steel cladding acting as initiation sites for intergranular attack was evaluated by exposing indented stainless steel coupons to a buffered Cs,Te mixture under conditions known to produce deep intergranular attack in cladding alloy. It was rationalized that both scratches and indentations would produce essentially the same surface effect, namely, localized areas of heavy cold work. Since highly deformed regions on the surface of nickel base superalloys have been shown to act as preferred sites for hot corrosion (oxidation-sulphidation)[26], it was obviously desirable to check whether similar features would play a similar role in fuel-cladding chemical interaction.

An annealed Type-316 stainless steel coupon specimen was indented at two different points with a spring-loaded center punch, then exposed for 100h at 725°C to a 1:1 Cs,Te mixture in a Cr,Cr_2O_3,C buffer. Figure 9 shows the specimen after light etching to reveal the unattacked grain structure. The distribution of attack indicates that the cold-worked region of alloy immediately

under an indentation (see left hand indentation) has only a minor influence on the depth of Cs,Te intergranular penetration. The maximum depth of penetration immediately below the righthand indentation is slightly greater than below adjacent nonindented surfaces, but this difference only appears to mirror the depression of the original surface at the site of the indentation. Uniform or matrix attack of the cladding is enhanced directly beneath the indentations, which is consistent with a higher density of carbide precipitation sites in heavily cold-worked regions. This enhancement of matrix reaction is illustrated in the high magnification photomicrographs comprising Figure 10. Detailed metallographic examination of indentations made on annealed Type-316 stainless steel blanks demonstrated that the indenting process did not cause cracks to develop in the alloy matrix.

E. EFFECTS OF COMMON FABRICATION IMPURITIES (Al, Si, Ca and C)

Silica, Alumina and Calcia. At HEDL, a series of laboratory capsule tests were conducted to assess the effects of calcium aluminate and silica impurities on fuel-cladding compatibility.[27a] Silica and calcium aluminate phases are

AS-POLISHED   (a) AFTER ATTACK   (b) AFTER ATTACK   100X

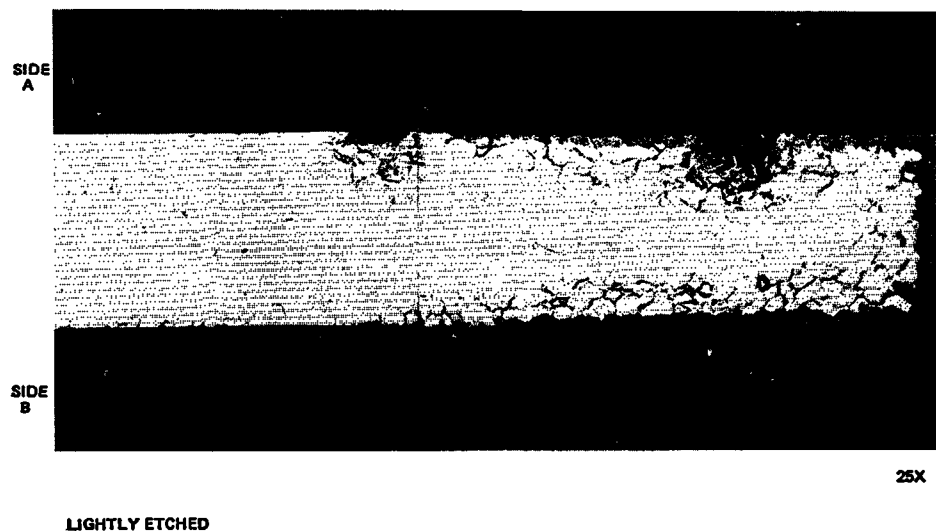100X   LIGHTLY ETCHED

SIDE A

SIDE B

25X

LIGHTLY ETCHED

Figure 9   Photomicrograph of Intergranularly Attacked Type-316 Stainless Steel Coupon Specimen Illustrating Effect of Surface Indentations

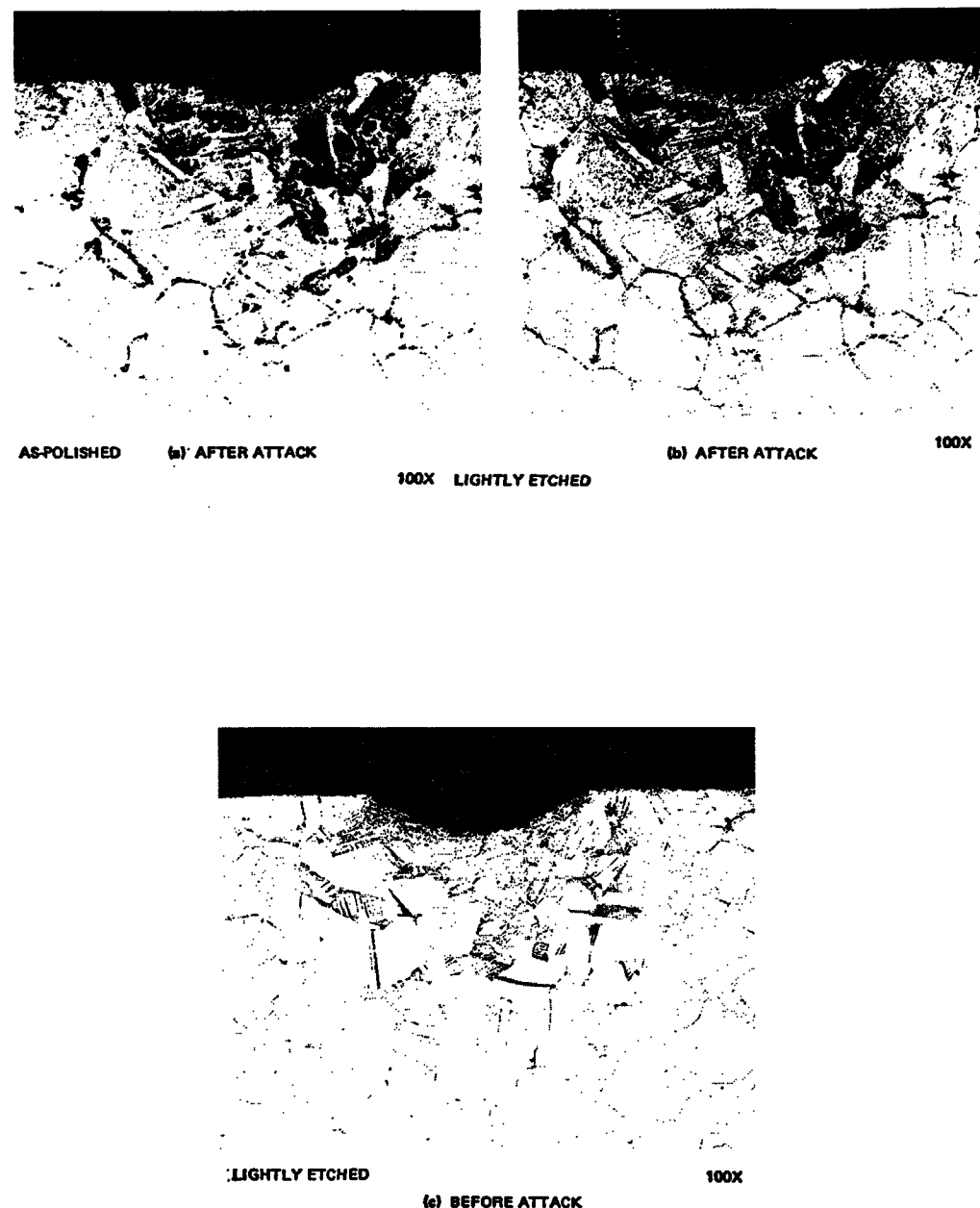;LIGHTLY ETCHED   100X

(c) BEFORE ATTACK

Figure 10   Photomicrographs of Surface Indentations in Type-316 Stainless Steel Coupon Specimen Before and After Attack by Cs, Te Mixture

occasionally observed as impurities in mixed-oxide fuels, their origins being thought to be the oxide refractories used in sintering furnaces. The specific purposes of the HEDL study were:

1) To provide data on the mobilities of Si, Ca and Al from SiO_2 and $CaO \cdot Al_2O_3$ fuel impurities to the cladding in an irradiated fuel pin, and

2) To determine possible effects of Si, Ca and Al on Cs, Te - induced FCCI at oxygen potentials corresponding to stoichiometric fuel.

Stainless steel capsules of the type shown in Figure 7 were fabricated to provide double containment of mixed-oxide fuel-cladding assemblies. The capsule assemblies in which a fixed orientation of the pellet-cladding assembly was maintained, were heat treated outside a glovebox. Silica and calcium aluminate impurities were introduced by application of slurries onto the fuel pellet surfaces, followed by high temperature treatments to stimulate chemical interaction (Pu silicate and Pu aluminate phases formed). The tests were performed at 600 and 800°, for 100 h and 1000 h.

The cladding attack depths resulting from these tests were typically 0.5 mil, and were less than 1 mil in all capsules. No evidence was found to indicate significant aggravation of FCCI by either silica or calcium aluminate. Silicon from silica-doped fuel was found to be mobile at 800°C, and became associated with Cs and Mn in the fuel-cladding gap. Calcium aluminate was stable and did not show any tendency to migrate from the fuel.

Carbon. Isothermal capsule experiments performed at GE [3] showed earlier that carbon, which is an unavoidable impurity in oxide fuel, markedly accelerates Cs, Te - induced intergranular attach of Type-316SS cladding in the "low" oxygen activity regime ($Po_2 \cong 4.6 \times 10^{-30}$ to ca 5.6×10^{-29} atm). In contrast to this, the same impurity was found to have essentially no influence on the intergranular attack rate either at higher oxygen activities ($Po_2 > 5.6 \times 10^{-29}$ atm) or in the absence of Te. Also, variations in the as-fabricated carbon level in typical austenitic cladding alloys (0.02 to 0.1wt per cent) has not been found to be a significant factor in determining depth of intergranular attack.

More recent capsule experiments have provided additional information about carbon impurity catalysis of Cs, Te - induced attack at "low" (VO/V_2O_3) and "intermediate" oxygen activities [22]. Details of these experiments may be found in Table 2 (section IV-B). At "low" oxygen activities the

catalytic effect of carbon was readily apparent (see Figure 8); in the absence of carbon the maximum intergranular penetration depth was 5.7 mils (145 μm), and in its presence the maximum penetration was 8.6 mils (218 μm). At "intermediate" oxygen activities the maximum penetration depths were smaller but less differentiated - 4.7 mils in the presence of carbon, 4.4 mils in its absence. It was also evident that whereas the deepest intergranular penetration tended to be localized in the absence of carbon, it was quite uniformly distributed over the cladding inner surface when carbon was present. This latter observation suggests that localized cladding inner surface precarburization might be important at "intermediate" oxygen activities.

Attempts to measure the movement and distribution of impurity carbon in Type-316 stainless steel during intergranular attack by Cs, Te(C) mixtures have been made using C-14 labelling and special autoradiographic techniques. In the initial experiments two Type-316 stainless steel capsules were exposed to Cs, Te mixtures (Cs: Te = 1:1) containing high specific activity carbon-14 (17 mCi/g). The stainless steel capsules used in the test were previously heat treated in vacuo at 1150°C for 1/2h to increase the average grain diameter to about 70 μm. To serve as a control sample one empty heat-treated Type-316 stainless steel capsule was placed alongside the two fission-product-filled capsules during their subsequent 725°C/200h heat treatment in argon. It was hoped that the autoradiographic technique employed would be capable of distinguishing between carbon concentrations in the grain boundary reaction phases and the normal distribution of carbon in slightly carburized cladding. The form of addition of Cs and Te was different in the two test capsules: in one, only Cs, Te and C were placed inside the test capsule which stood open inside a slightly larger, sealed, Type-316 stainless steel capsule containing a Cr/Cr_2O_3 buffer mixture. The other capsule contained an intimate Cs, Te, Cr, Cr_2O_3,C mixture and was sealed. The three capsules were placed together inside an evacuated Vycor ampoule for the 725°C heat treatment. After completion of the tests, longitudinal metallographic sections from near the bottom end caps of each capsule were prepared in the as-polished condition. These sections were then photographed and attacked areas autoradiographed. The photomicrograph and matching auto-radiograph shown in Figure 11 are from a selected area of the capsule containing the Cs, Te, ^{14}C mixture. In this capsule the maximum observed inter-granular penetration into the stainless steel was 8.0 mils (202 μm), i.e., approximately 3 grain diameters. Comparison of the C-14 autoradiograph and the optical photomicrograph shows that there were high concentrations of

C-14 in the attacked grain boundaries but not in the unattacked grain boundaries. The autoradiograph also showed that carbon-14 had become uniformly distributed throughout the matrix of the cladding alloy during the time of the test (200h). From these two observations it appears that the carbide grain boundary phases were precipitated before significant quantities of impurity carbon had diffused into the stainless steel specimens. Earlier studies of carbide precipitation in annealed Type-316 stainless steel cladding samples showed that significant quantities of carbide precipitates formed in the grain boundaries within 10 hours at 725°C.[3]

A second set of experiments was performed in which Type-316 stainless steel coupon specimens containing carbon-14 presegregated in the grain boundary carbides were chemically attacked by a variety of simulated fuel-fission product (Cs, Te) mixtures. The carbon-14 doped Type-316 stainless steel specimens were prepared in the following manner: 1x2x13 mm coupons were cut from polished wafers of annealed Type-316L stainless steel bar stock (two different grain sizes), then reacted with a predetermined amount of C-14 labeled methane gas at 600°C in a special gas-handling system. The samples were then placed inside a sealed Type-316 stainless steel capsule filled with argon which was heat treated at 2100°F (1148°C) for 1/2h to homogenize the added carbon.
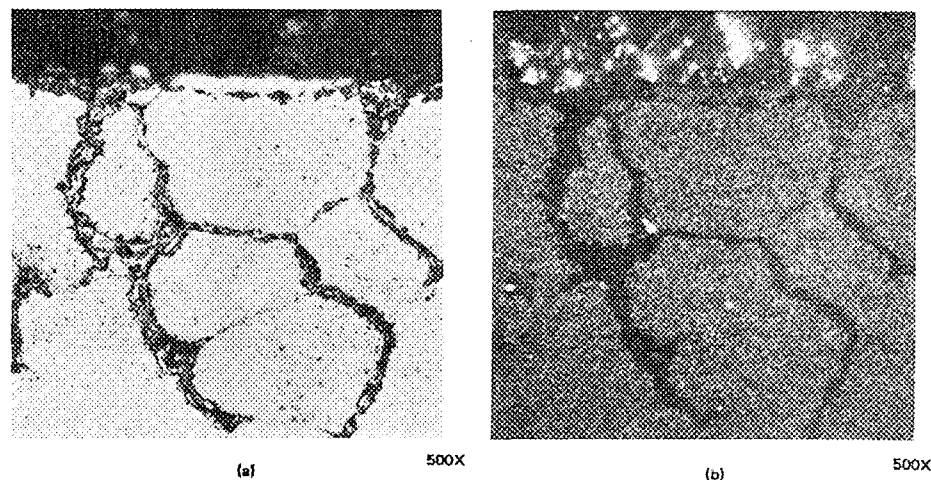

(a)   500X   (b)   500X

Figure 11 *Distribution of Carbon (Plate b) in Intergranularly Attacked Type-316 Stainless Steel. Plate (a) is an As-Polished Photomicrograph Showing the Intergranular Attack Morphology; Plate (b) is a Darkfield Photograph of the Autoradiographic Emulsion After a 168h Exposure to the Area Shown in (a)*

Next, the samples were heat treated at 1300°F (703°C) for 100 hours to precipitate a portion of the labelled carbon as grain boundary carbides. Following this "sensitization" treatment the samples were exposed to a variety of Cs, Te mixtures to obtain varying degrees of intergranular attack (10 and 100 hours at 725°C, with and without $Cr/Cr_2O_3/C$ buffer). One stainless steel coupon (34-1) was given a 100h/725°C heat treatment 'in vacuo' to provide a control specimen for parallel metallographic, autoradiographic, and scanning electron microprobe (SEM-EDAX) examinations.

Two attacked specimens (34-2 and 34-4) were selected for detailed examination. Each specimen showed extensive grain boundary penetration; however the maximum penetrations were different due to the different grain sizes. As-polished photomicrographs of these two specimens are shown in Figure12 , the numbers on these photomicrographs refering to grain boundary locations that were subjected to detailed scanning electron microscope (SEM) examination. Soft beta autoradiographs of the control specimen and the attacked specimens showed carbon concentrating on all the grain boundaries in the control specimen but carbon activity only appeared on the unattacked or least attacked grain boundaries in the attacked specimens. The resolution of the autoradiographs left something to be desired, being limited by the thickness of the radiographic emulsion. From these results it was inferred that carbon originally combined as carbide in the grain boundaries was removed from or depleted in the chemically attacked regions.

To provide additional information about the role of carbon/grain boundary carbides in the accelerated Cs, Te intergranular attack mechanism, attempts have also been made to photograph and microprobe-analyse carbide particles in attacked and unattacked grain boundaries of the C-14 doped Type-316 stainless steel coupon specimens (34-1, 34-2, and 34-4). The stainless steel alloy matrix in the vicinity of grain boundaries was selectively removed from prepared metallographic samples using an electrolytic etch technique originally developed by Maiya et al. for Type-304L stainless steel[23]. In this technique the specimens are immersed in a 5 vol% solution of HCl in methanol while a current of density 500mA/cm^2 is passed for 15 to 60 seconds. As illustrated in Figure 13, this treatment reveals the feathery (dendritic) carbide particles that reside in the normal grain and twin boundaries of "sensitized" Type-316 stainless steel by selectively removing the matrix alloy in the immediate vicinity of intragranular particles. The transmission electron microscope study previously referenced had shown that both the inter- and intragranular precipitates in these Type-316 stainless steel specimens were $M_{23}C_6$-type carbides.[3]

A series of SEM photomicrographs from progressively deeper locations on the grain boundaries of the selectively-etched (attacked) Type-316 stainless steel specimen 34-2 are shown in Figure 13. The complete absence of grain boundary particles in the heavily etched section of the first grain boundary

CAPSULE 34-2   100X

TILT, 0°   1000X
(a) HIGH MAGNIFICATION OF LOCATION 1

CAPSULE 34-4   100X

TILT, 0°   1000X

(b) ATTACKED GRAIN BOUNDARY TO LEFT OF
AND SLIGHTLY BELOW LOCATION 2 (2a)

                                                                3000X

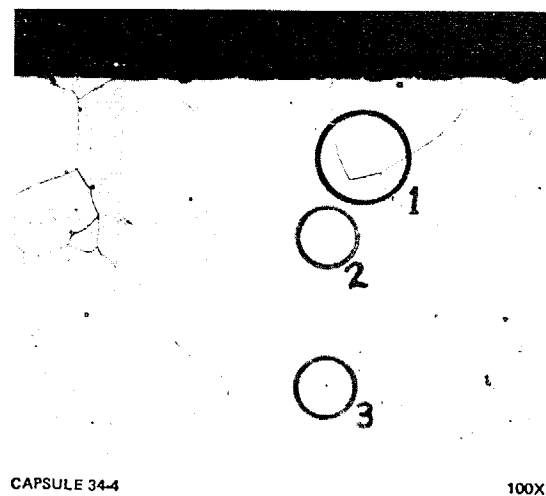(c) UNATTACKED GRAIN BOUNDARY AT LOCATION 4 (34-2)

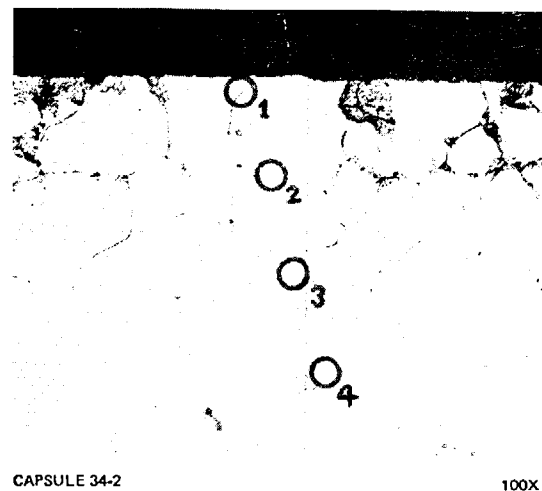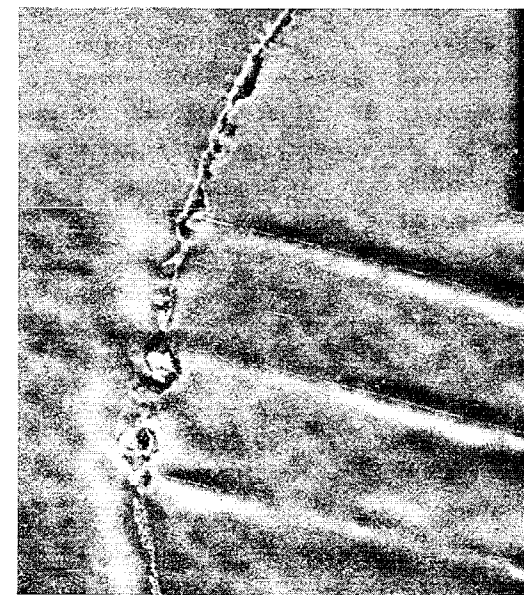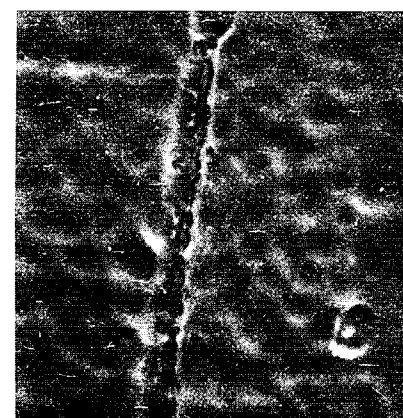*Figure* 12 *Optical Photomicrographs of C-14 Doped 316 Stainless*
Steel After Intergranular Attack by Cs, Te-Mixtures at 725°C

Figure 13 *SEM Photomicrographs of Attacked Type-316 Stainless Steel — Specimen 34-2*

is notable, as is the presence of a virtually intact layer of intergranular particles in the unattacked (lower) section of the same grain boundary. Plate (b) shows a moderately etched grain boundary to the left of, and slightly below, location 2. Although particles are still visible in this grain boundary, their degraded condition, which is worse than in the previous lightly etched grain boundary, indicates they had undergone extensive reaction/dissolution. Plate (c) shows details of an unattacked (non-etched) grain boundary at location 4; here the dendritic carbide particle structure is identical to that observed in the control specimen. Similar observations were made on the other attacked specimen (34-4).

Using the SEM beam as an electron microprobe, some characteristic x-ray fluorescence spectra were obtained for adjacent intergranular precipitate and matrix regions. Although no differences in the (metallic) composition of attacked and unattacked grain boundary particles could be detected, an enrichment of chromium relative to iron in the precipitates was easily recognized. The observed physical degradation of the grain boundary particles as Cs, Te-induced attack progresses is believed to correspond to chemical conversion of the chromium-rich carbide particles to chromium-rich oxide:

$$(M_{23}C_6, M_7C_3 \text{ etc}) + [O]_{Cs,Te} \rightarrow M_2O_3 + C$$
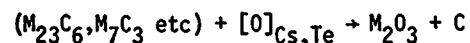
(In this model the integrity of the particle layer is not expected to break down until all the carbide has been oxidized and the oxide product has started to dissolve in the (liquid) Cs,Te "flux".) Thus far direct evidence that particle degradation corresponds to carbide→oxide conversion has not been obtained.

Silicon Carbide. Fuel pellet grinding procedures are a potential source of silicon carbide contamination inside fuel pins. A recent out-of-pile study at HEDL [27] has provided information on the influence of SiC particles in the fuel-cladding gap on Cs,Te-induced FCCI. The method employed to obtain this information was the same as that described earlier in this section (for example, see Figure 7c). SiC particles were found to cause local intensification of cladding chemical attack at 800°C but not at 600°C. The mechanism by which this occurs is believed to involve partial oxidation of SiC to SiO/SiO$_2$ with release of carbon. This carbon then catalyses Cs,Te-induced intergranular attack of the cladding.

F. EFFECTS RELATED TO COMPOSITION AND INVENTORY OF FISSION PRODUCTS

Composition of Cs,Te Mixtures. The critical dependence of the *incidence* of Cs,Te-catalysed attack of Type-316 stainless steel on Cs:Te ratio was realized early in the GE test program [3]; however, details of the dependence of attack *morphology* on composition have only recently been obtained. Isothermal capsule tests were used to obtain these data and, in each case, the quantities of fission products used were considerably in excess of those expected in an equivalent length of an irradiated fuel pin. Table 5 summarizes the results of these tests.

Tellurium alone was found to produce either a characteristic shallow mixed uniform-intergranular attack (1-2 mils) or essentially no attack at "low" oxygen activity levels. Two representative Te activities were obtained by varying the Cr:Te ratio in the Te-buffer mixture. Absence of cladding attack was associated with low Te activity (Cr:Te = 4:1) whereas "high" Te activity (Cr:Te = 1:2) produced attack. Electron microprobe measurements indicate that the uniform reaction layer in the Te-attacked 316-SS specimens consists of two different tellurides: (Cr,Ni,Fe) Te$_2$ (outer) and (Fe,Ni)$_{1-x}$ Te (inner).

Table 5. Effect of Varying Fission Product Composition
(Test Conditions — 100h at 725°C; Cr/Cr$_2$O$_3$/C Buffer)

Cs:Te Ratio	Conditions	Result/Observation
0:1	Low PO$_2$, low a$_{Te}$	No attack (<0.25 mil)
0:1	Low PO$_2$, high a$_{Te}$	Combined attack (∿2 mils)
0.2:1	Low PO$_2$, low a$_{Te}$	Intergranular attack[†] (∿4 mils)
0.2:1	Low PO$_2$, high a$_{Te}$	Intergranular attack[†] (∿4 mils)
1:1	Low PO$_2$	Intergranular attack (4-5 mils)
2:1	Low PO$_2$	Intergranular attack (4-5 mils)
3:1	Low PO$_2$	Predominantly IGA (4 mils)
4:1	Low PO$_2$	Uniform/matrix attack (∿2 mils)
8:1	Low PO$_2$	No attack
0:1	Low PO$_2$	No attack, shallow carburization

[†]Deep IGA only observed where Cs present.

The effect of adding a relatively small amount of Cs to tellurium is dramatic. The added cesium was insufficient to change the Te activity via a mass action effect (i.e., $2Cs+Te=Cs_2Te$), and it was added to the other capsule contents as a single drop with the capsule slightly tilted just prior to sealing the capsule. This mode of addition ensured that the cesium would not be uniformly distributed on the inner surface of the cladding. Figure 14 shows that deep intergranular penetration of the cladding only occurred where the cesium was present; the remaining areas show attack characteristic of tellurium alone. Attempts to vary Te activity in these capsules by changing the Cr:Te ratio did not have any effect on the incidence of deep intergranular attack. This indicates that the Cs,Te-induced intergranular attack process is relatively insensitive to Te activity over a considerable range.

AS-POLISHED　　　　(a) Cs:Te ~ 3:1　　　　250X

AS-POLISHED　　　　(b) Cs:Te ~ 4:1　　　　250X

100X
(a) LOCATION WITHOUT Cs (Te ALONE)

100X
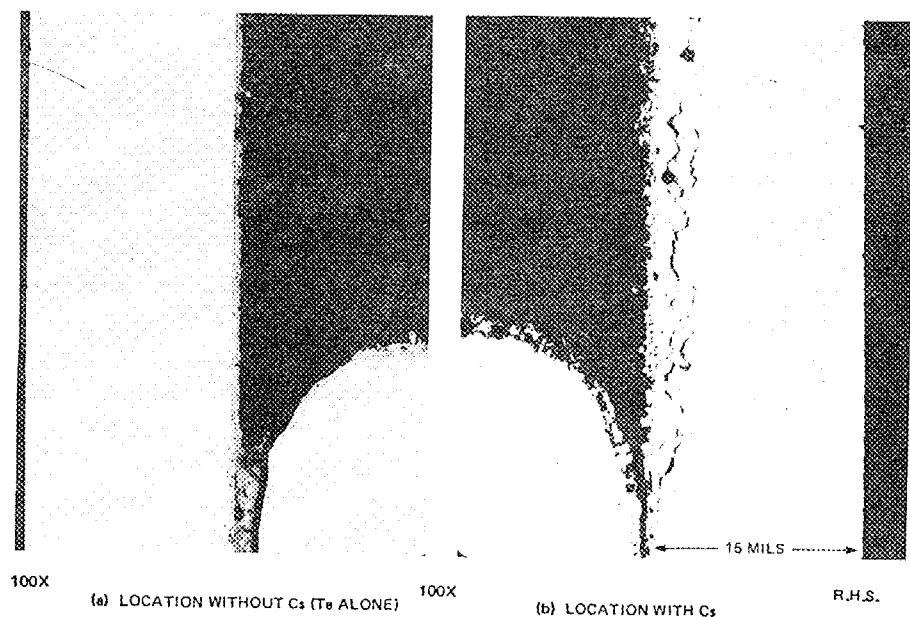(b) LOCATION WITH Cs

15 MILS

R.H.S.

Figure 14 As-Polished Photomicrographs of Intergranularly Attacked Sections of 316 Stainless Steel Cladding Alloy Taken From Opposite Sides of Capsule
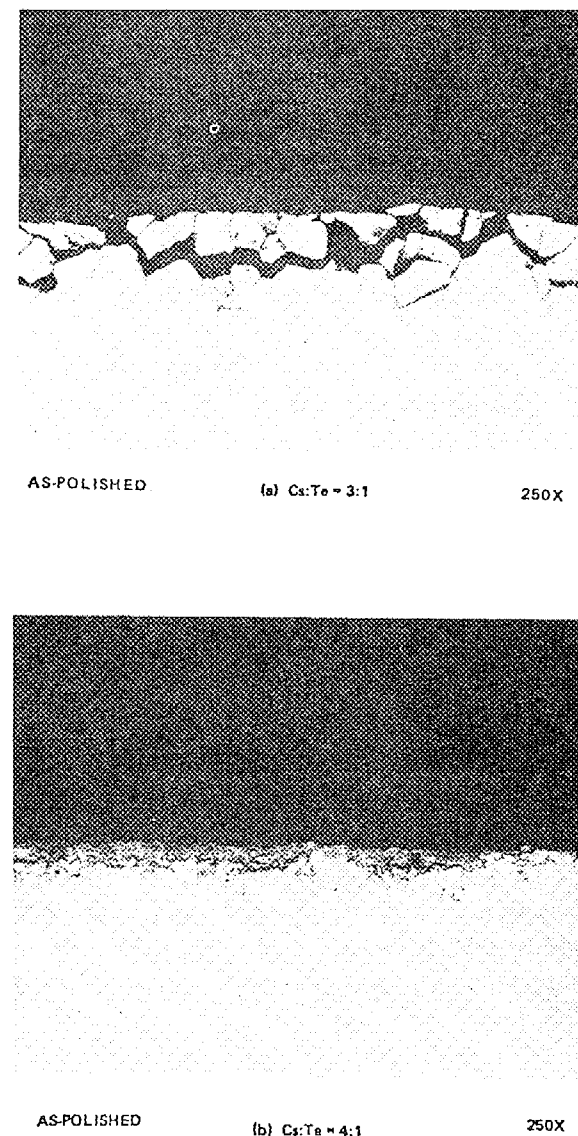
Figure 15 Photomicrographs of Annealed Type-316 Stainless Steel Samples After Exposure to Cs, Te-Mixtures at Low Oxygen Activity Showing Effect of Cs:Te

The tests performed at higher Cs:Te ratios showed that Cs,Te-induced inter-granular attack at "low" oxygen activity (Cr/Cr$_2$O$_3$/C buffer) occurs when Cs:Te$\leq$3:1. Between Cs:Te=3:1 and Cs:Te=4:1 the character of attack changed from predominatly "intergranular" to a shallower "uniform" attack; these differences are illustrated in Figure 15. With Cs:Te=8:1 no attack was observable, a result which implies that a mass action effect of Cs on Te activity is operative. An absence of attack was also noted with Cs alone, however a general darkening of grain boundary regions on the cladding inner surface, as revealed by light electrolytic etching, indicated that local carburization had occurred. This observation supports earlier results[1], which suggested that liquid cesium(or liquid Cs-Te alloy) could act as an effective transport medium for carbon impurity, i.e., either from the fuel to the cladding or between phases in (attacked) cladding grain boundaries.

Availability of Cs+Te (Inventory Effects). Consumption of Cs and/or Te during the intergranular attack process would require that their availability/supply rate at the cladding inner surface controls the overall rate of grain boundary penetration. Since very little infor-mation on this particular aspect of the intergranular attack mechanism was available a series of experiments was initiated at GE to determine whether intergranular attack depth depended on the quantity of Cs+Te accessible to a given surface area of cladding material. [22]

A variety of experimental arrangements incorporating sandwich-configuration stainless steel specimens are being tested in the GE program. Typically, in these sandwich-configuration arrangements,a limited quantity of fission products (2-30 mgm Cs$_2$Te powder) is placed into a flat-bottomed cavity in a cylindrical piece of annealed Type-316 stainless steel and held in place by a pellet of buffer material (Cr,Cr$_2$O$_3$,C) or fuel (UO$_{2.00}$) or Type-316 stainless steel. In the latter case a fixed quantity of oxide buffer is mixed with the Cs,Te additives to provide an adequate supply of oxygen. Several of the sandwich specimens are stacked on top of each other and sealed inside argon-filled nickel capsules for the heat treatments (725°C/ 100 hours or 200 hours). This type of arrangement is illustrated in Figure 16 together with a typical metallographic section of an attacked Type-316 stainless steel sandwich specimen. The early tests performed with UO$_2$ and Cr$_2$C$_3$,Cr$_2$O$_3$ pellets only produced a shallow ($\sim$1 mil) uniform oxidation of the stainless steel surfaces and no differentiation between the attack depths in the various samples. Better results were obtained

with Cs$_2$Te, Cr-Cr$_2$O$_3$-C mixtures sandwiched between two stainless steel surfaces, and a clear proportionality between maximum attack depth and quantity of Cs$_2$Te was revealed. The results from one of these series of tests are presented in Table 6.

Table 6
INTERGRANULAR ATTACK OF TYPE-316 STAINLESS STEEL BY LIMITED QUANTITIES OF Cs+Te

Test Conditions	100h at 725°C
Buffer Mixture	Cr,Cr$_2$O$_3$,C
Total Exposed Surface Area of Type-316SS	ca. 1 cm^2

	Quantities of Additives (micromoles)				
Specimen No.	Cs$_2$Te	Cr	CrO$_{1.5}$	C	Results
32R-1	56	37	70	83	Intergranular Penetration, 2.5-3.0 mils/63-76 μm
32R-2	39	37	70	83	Intergranular/Pitting Attack, d$_{max}$~0.75 mil/19 μm
32R-3	28	37	70	83	Intergranular/Pitting Attack, d$_{max}$~0.75 mil/19 μm
32R-4	14	37	70	83	Intergranular Penetration, d$_{max}$~0.5 mil/13 μm

Unfortunately the differences between the measured penetration depths in these type of specimens were not sufficiently clear-cut to permit an accurate determination of the functional dependence of depth of penetration of "quantity of Cs$_2$Te". Difficulty in retaining the Cs+Te mixtures on the flat stainless steel surfaces during testing, and a deterioration in the quality of the Cs$_2$Te source contributed to this lack of resolution. A modification of this particular approach, in which the fission product-buffer mixtures are actually sealed inside the 316SS sandwich, is ex-pected to improve the precision of the results.

Additional evidence that the maximum Cs,Te-induced intergranular attack depth in Type-316 stainless steel depends on the availability of Cs+Te was also obtained from a series of isothermal capsule experiments in which progressively larger quantities of high purity Cs$_2$Te were added to a fixed amount of VO,V$_2$O$_3$ buffer. It was apparent from the results that deep Cs,Te-induced intergranular penetration does not commence until some critical quantity of Cs$_2$Te is reached and thereafter the attack depth tends to in-crease as Cs$_2$Te is added. The design of these experiments was such that the precise quantity of Cs+Te reaching the cladding inner surface could not be determined, however an upper limit for the "threshold" quantity was estimated to be 2.4 mgmTe/cm^2 (note:the affected internal surface area

these capsules is ca. 1.6 cm^2). This figure is in the same range as the Te concentrations found to cause attack in the sandwich specimen (1.8 to 7.2 mgm/cm^2; the lowest figure in this range is equivalent to the expected cladding coverage in a mixed oxide fuel rod at 10 atom% burnup assuming all the Te fission products deposit uniformly on the cladding surface). An interesting observation from these isothermal capsule experiments was that, in the presence of carbon impurity,observable IGA (i.e. $\geq$ 1 mil) was initiated at a somewhat lower Cs+Te concentration than in its absence. In view of the known catalytic role of carbon in the Cs,Te-induced intergranular attack process [3], such an effect is expected.

G. EFFECTS OF OTHER "AGGRESSIVE" FISSION PRODUCTS

In common with investigators in other countries,workers in the US have found that, out of the approximately 30 fission product elements present in irradiated fuel, only Cs, Te, Se, Br and I are capable of undergoing significant chemical interactions with the cladding material of an LMFBR fuel rod. In irradiated oxide fuel pins, iodine (and bromine) fission products normally combine with cesium (and Rb) fission products to form CsI (CsBr), a compound which is thermodynamically stable with respect to possible Cs-fuel, Cs-cladding or Cs-fission-product compounds except at very high oxygen activity levels [28,29]. Tellurium (and, presumably selenium) fission products also form stable compounds with the relatively plentiful Cs fission products (e.g., Cs$_2$Te) but, unlike CsI, these compounds undergo vigorous chemical reaction with austenitic stainless steel cladding at the (low) oxygen activities that correspond to hypostoichiometric fuel. Although the high oxygen activity levels necessary to release iodine from CsI (PO$_2$ $>$ 1x10^{-11} atm at 700°C), thereby making it available for direct reaction with the cladding, far exceed oxygen activities expected to develop in the fuel-cladding gap of a pin containing initially hypostoichiometric fuel it was considered prudent to evaluate CsI as a potential cause of FCCI. This was done by performing a series of Type-316SS isothermal capsule experiments at 725°C/ 100 h with Cs:CsI ratios covering the range 0:1 to 4:1. [22] The oxygen activity level in the capsules was controlled using both stoichiometric UO$_2$ and Cr, Cr$_2$O$_3$, C buffer mixtures and great care was taken to exclude moisture. Cesium iodide itself did not attack the Type-316 stainless steel at either oxygen activity level, in the presence or absence of carbon. However, in the presence of Cs (Cs:CsI=2:1 to 4:1) shallow pitting of the cladding surface occurred in some areas (<1 mil). At certain Cs:I ratios, with carbon present in the Cs+CsI mixture, the cladding was carburized in regions

where it made contact with the fission product melt. When Te was deliberately added to the Cs+CsI mixtures, such that the ratio of Te to "free" Cs remained above 1:3, deep intergranular attack of the cladding resulted ($\geq$5 mils/127um).
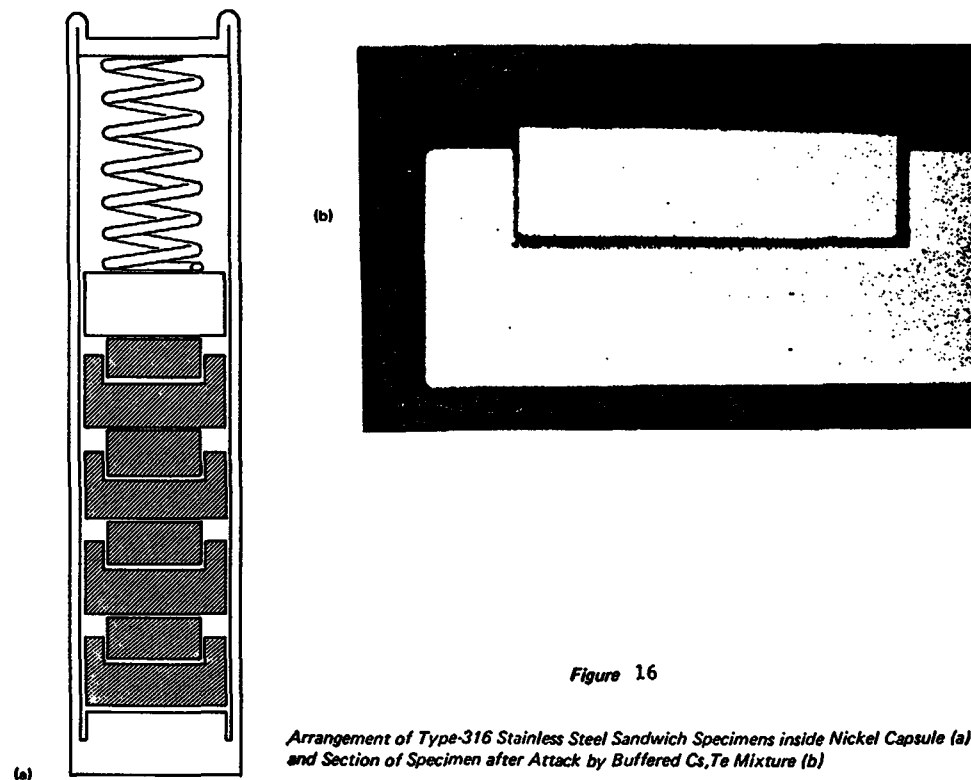

(b)

(a)

Figure 16

Arrangement of Type-316 Stainless Steel Sandwich Specimens inside Nickel Capsule (a) and Section of Specimen after Attack by Buffered Cs,Te Mixture (b)

Molybdenum, in close association with cesium, is found in regions of fuel-cladding chemical interaction. The mechanism of transport of Mo from the fuel into the attack zone is generally acknowledged to involve Cs$_2$MoO$_4$(v) which, depending on local conditions of temperature and oxygen activity, may form over hot regions of the fuel.[3,30] Although (liquid) cesium molybdate has been proposed as an essential constituent for fission-product-induced cladding intergranular attack [2], isothermal capsule tests performed at 650°[29] and 725°C[3] have shown that either alone or in the presence of cesium, Cs$_2$MoO$_4$ does not promote intergranular attack in Type-316 stainless steel. The primary influence of Cs$_2$MoO$_4$ on fuel-cladding chemical interaction thus appears to be through its effect on Cs and oxygen availability.

H. SUSCEPTIBILITY OF ALTERNATE CLADDING ALLOYS TO FCCI

In the United States a number of alternative alloys to 20% CW 316SS are actively being considered as possible advanced cladding materials. As part of a large national program to develop and characterize these various alloy types,an initial out-of-pile scoping study of the degree of chemical interaction undergone by different alloys in a fuel-fission product environment known to be aggressive towards the present reference cladding alloy (20% CW ·316 SS) was performed[25]. The technique employed was essentially the same as that being used to characterize the fission product-induced attack process in the 300 series stainless steels (304, 316, 321 and 347)[3,22] that is, exposure of coupons of the various alloys to buffered Cs,Te mixtures (see Figure 7, b). The alloys were screened at two representative temperatures (650 and 725°C) at "high" (Fe/FeO/(C)) and "low" ($Cr/Cr_2O_3/(C)$) oxygen activity levels. Excess quantities of the fission product additives, Cs:Te=1:1, were also used to maximize the degree of chemical interaction that occurred in a given time period (24-400 hours). It was recognized at the very outset of this investigation that certain alloy types would probably exhibit quite different attack characteristics (and mechanisms) to Type 316 austenitic stainless steel. For example, a ferritic alloy could prove to be more susceptible to Cs,Te-induced oxidative attack at "high" oxygen activities than at "low" oxygen activities (the reverse of 316 SS behavior), and the grain boundary carbide precipitation rates in certain high Ni alloys could influence their susceptibility to carbon catalysis of an intergranular mode of attack. Also, the wide variations in main constituent composition (i.e., % Cr) of the alloys screened could also change the oxygen activity threshold for a particular type of attack in a particular alloy at a given temperature.

The study showed that the degree and type of attack suffered by the different alloys depended on the oxygen activity, temperature, availability of carbon impurity and, in certain alloys, carbide precipitation kinetics. Based on the scoping test results, the following conclusions were drawn:

1) After allowance for grain size effects (see next section), the depth of intergranular attack in different austenitic alloys at low oxygen activity ($Cr/Cr_2O_3/C$ buffer) was found to decrease with increasing nickel content of the alloy. These results are illustrated in Figure 17.

2) At high oxygen potentials (Fe/FeO/C buffer), the extent of mixed (intergranular-matrix) attack showed a general increase with increasing nickel content of the alloy.

3) Catalysis of Cs,Te-induced attack by impurity carbon appeared to be important in a number of alloys.

4) An initial induction period in the Cs,Te-induced attack of PE-16, 330SS, I-901 and HT-9 at low oxygen activity (725°C) appears to be related to carbon diffusion and carbide precipitation kinetics.

5) In most alloy specimens as-cut (cold-worked) surfaces were attacked to approximately half the depth that polished surfaces were attacked.

I. CLADDING MICROSTRUCTURAL EFFECTS

During the course of the systematic laboratory investigation at GE several observations were made on the effect of grain size variations, in 316, 321 and 347 stainless steel samples on resulting attack depth by Cs,Te mixtures.[25] In 725°C/100 h tests, the intergranular penetration depth was found to increase almost linearly with increasing grain size of the cladding samples (i.e., the effective grain boundary area exposed to the corrodants for a given time decreases with increasing grain size). Workers at ANL made similar observations for intergranular penetration of a variety of 300-series austenitic alloys (304,316, 318) by liquid cesium oxides[23]. On the basis of these results, a linear correlation between intergranular attack depth and grain size was assumed and used to normalize the FCCI results from alternate cladding alloys (section III-H).

Significant differences have not been observed in the rates of penetration of Cs,Te mixtures into solution-treated Type-316 SS and Type-316 SS sensitized by aging at 725°C for various times prior to a fission product compatibility test. This apparent insensitivity of intergranular penetration rate to initial carbide morphology results from the fact that carbide precipitation (sensitization) is quite rapid at test temperatures in the range 650-800°C. Generally, by the time cladding attack measurements have been made (20-50h), carbides precipitates are well-developed in the grain boundaries of initially solution-annealed Type 316 SS. Similar experiments at ANL have shown that the presence of intergranular carbide precipitates is not necessary for grain-boundary penetration of Type-304 SS by cesium oxide at 450°C[23].

The effects of long term aging of austenitic cladding alloys (316 SS and PE 16) in the temperature range 700-815°C on subsequent FCCI behavior is presently being investigated at GE. Long term aging of the US reference cladding alloy in this temperature range is known to produce intermetallic second phases such as sigma and chi, and it is desired to evaluate the consequences of their precipitation on cladding susceptibility to FCCI.
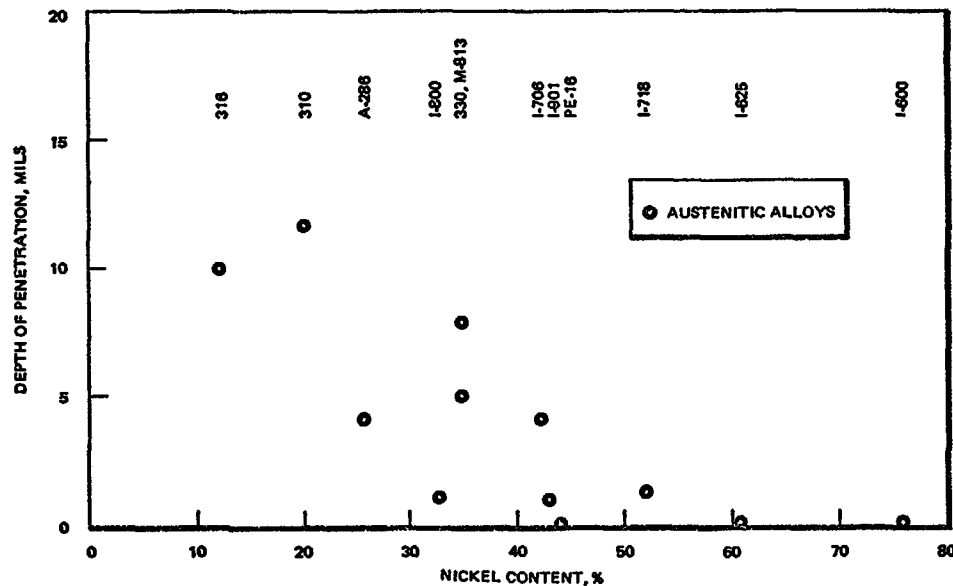
Figure 17 Depth of Penetration Normalized for Grain Size for Advanced
Alloys Exposed to Cr + Cr₂O₃ + C at 725°C for 400 Hours
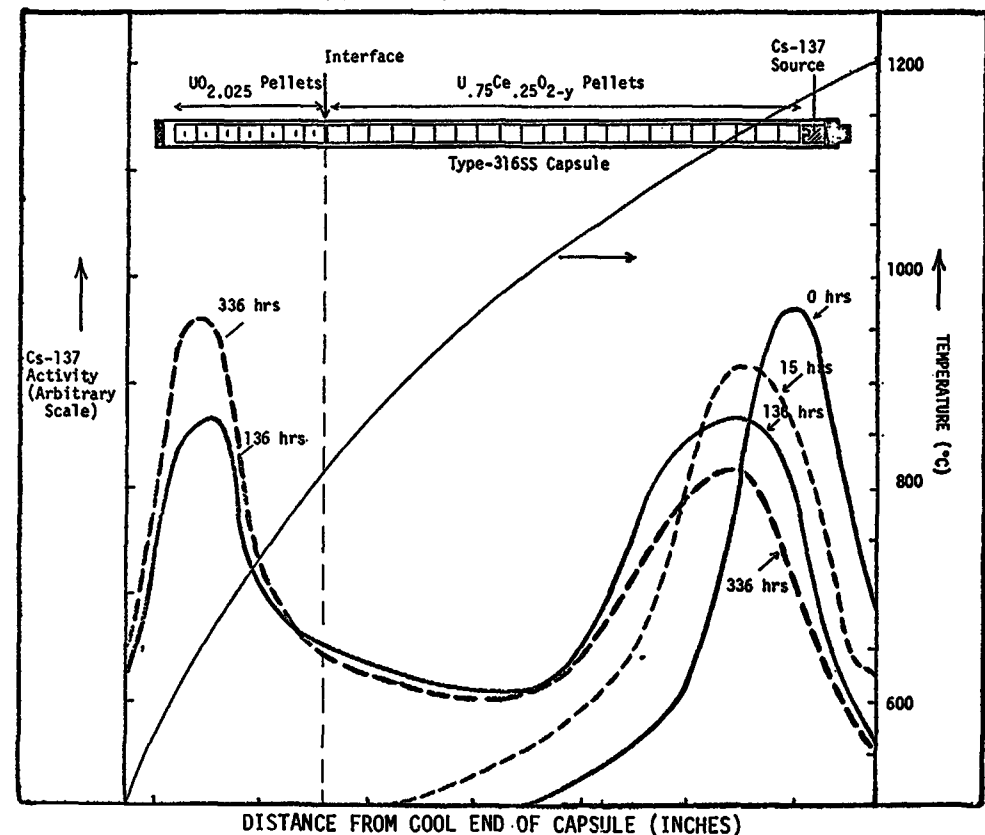
IV. TEMPERATURE GRADIENT TESTS

A. Cesium Thermomigration Experiments

Out-of-pile temperature gradient experiments have been performed in long
capsules to obtain rate data for Cs thermomigration along a mixed oxide
fuel column and to gain information about fuel swelling at mixed oxide-UO_2
interfaces due to Cs-fuel chemical interaction.[31] Experimental parameters
that were varied were fuel oxygen activity (O:M ratio), blanket oxygen
activity (O:U ratio) and temperature gradient (∇T). Mixed urania-ceria
($U_{.75}Ce_{.25}O_{2-y}$) pellets were used to simulate mixed oxide fuel, and two
different capsule designs were employed.One of these designs is illustrated
in Figure 18, which also shows the Cs thermomigration results. The
basic difference in designs was that longer molybdenum capsules were used
for the tests with the highest maximum temperature and steepest axial tem-
perature gradient. In each case the mixed oxide-UO_2 pellet interface was
located inside a length of Type-316 stainless steel cladding (pellet-clad
diametral gap ∿3 mils) at a position corresponding to a temperature of ∿800°C.
Two six-inch long stainless steel capsules were loaded with "low O.M" urania-
ceria pellets, hyperstoichiometric UO_2 pellets (O:U = 2.025) and a source of
cesium (ca. 50 mgm Cs metal, plus 50 μCi Cs-137), and two 8-1/2-inch long
molybdenum capsules were loaded with "stoichiometric" urania-ceria pellets,

stoichiometric UO_2 pellets and 50 mgm tagged Cs metal. Identical pairs of
capsules were used so that one capsule would be available for destructive
examination.

The heat treatments were performed inside a calibrated temperature
gradient furnace under purified argon. After each heat treatment, the
capsules were gamma scanned (Cs-137) to follow the progress of cesium
along the fuel column and to determine whether significant quantities of
Cs had reached the fuel-blanket interface. The compositions of the urania-
ceria pellets were previously adjusted to "low O:M (equivalent O:M in
urania-25% plutonia ∿ 1.94) and "stoichiometric" by equilibration at 1500°C
in flowing hydrogen. The evolution of the cesium gradients in one of the
test capsules is illustrated in Figure 18, which also shows the temp-
erature gradient and fuel pellet locations applicable to this capsule
design. The measured Cs gradients after a given annealing time were
identical for each of the capsules constituting a pair. More rapid

FIGURE 18 Cs THERMOMIGRATION RESULTS FOR SERIES IX CAPSULES NO. 3 AND NO. 4

DISTANCE FROM COOL END OF CAPSULE (INCHES)

movement of Cs down the temperature gradient in the "low O:M"/low ΔT capsules was immediately evident from the experimental Cs-137 profiles; however, the retention of significant quantities of Cs by the high temperature fuel after 128 hours was somewhat surprising. (It is suspected that inadvertent oxidation of the outer surfaces of the "low O:M" $U_{0.75}Ce_{0.25}O_{2-y}$ pellets during transfer and loading was responsible for the apparent Cs-fuel chemical interaction in the hot zone.) As observed in previous Cs thermomigration experiments,[1,3] transport of Cs down a temperature gradient was extremely slow (below $\sim 1000°C$) at average fuel O:M ratios greater than the threshold value for Cs-fuel chemical interaction (~ 1.985). Both of the "low O:M" capsules were destructively examined in the region of the blanket pellets where Cs had concentrated. Significant volumetric expansion of the $UO_{2.02}$ pellets had occurred at this location ($\Delta D/D_{max} \gtrsim 8\%$); however, concomitant cladding strain was only observed at certain orientations.

Research at GE and ANL has shown that the low density product of the Cs-fuel chemical interaction is Cs_2UO_4. However in the present experiments it did not form exactly at the fuel-UO_{2+x} interface, presumably because the blanket pellets had been reduced (to UO_2) by the low O:M fuel. One of the Mo capsules that contained "stoichiometric" fuel was sectioned at the $UO_{2.00}$-$U_{0.75}Ce_{0.25}O_{2.00}$ interface where Cs had concentrated after 1000 hours. No fuel pellet or blanket (UO_2) pellet swelling was evident at this location, even though the first blanket pellet contained a substantial fraction of the total Cs. Metallography performed on this pellet revealed that grain boundary etching had occurred but confirmed the absence of volumetric expansion.

B. **Mass Transport of Cladding Components by Cs-Te Fission Products**

In an attempt to characterize the cladding component (Fe,Cr,Ni) mass transport process that was identified in Cs,Te-doped mixed oxide fuel rods,[14] some radial temperature gradient experiments have been performed at General Electric.

In the annular capsule design (see Figure 19), a temperature gradient of approximately 75 degrees C was maintained between the inner and outer walls of two concentric Type-316 SS tubes, which space also contained a buffered Cs,Te mixture. The temperature gradient was achieved by positioning the capsule in the constant temperature zone of a tubular furnace ($\sim 675°C$) and passing a controlled current through the central resistance heater. Variables under study are Cs:Te ratio, oxygen activity, time and the presence of alloying metals such as molybdenum and niobium on the hotter stainless

steel surface. Essential test conditions in the completed experiments were: Cs:Te $\simeq$ 1:1, T_{min} = 700°C, time = 150-250 hrs, "low" oxygen activity (Cr/Cr_2O_3 buffer) and "intermediate" oxygen activity (NbO_2/Nb_2O_5 buffer). Metallographic examination of the capsule from a test performed at low oxygen activity showed no evidence of cladding component transport from either wall; neither was any intergranular attack observed. Results from a test performed at high oxygen activity showed more erosion/dissolution-type FCCI on the cooler wall, and some evidence of material deposition on the hotter wall. As-polished photomigrographs from this section of the capsule are illustrated in Figure 20 . SEM-EDAX measurements on the suspected deposits at this location showed that they were iron-rich (see Figure 20 b,c); however, because their composition was similar to that of the substrate, it could not be verified that their source was the cooler wall. Nb and Mo coatings on the surface of the hotter wall are presently being employed to eliminate ambiguity from this type of result.
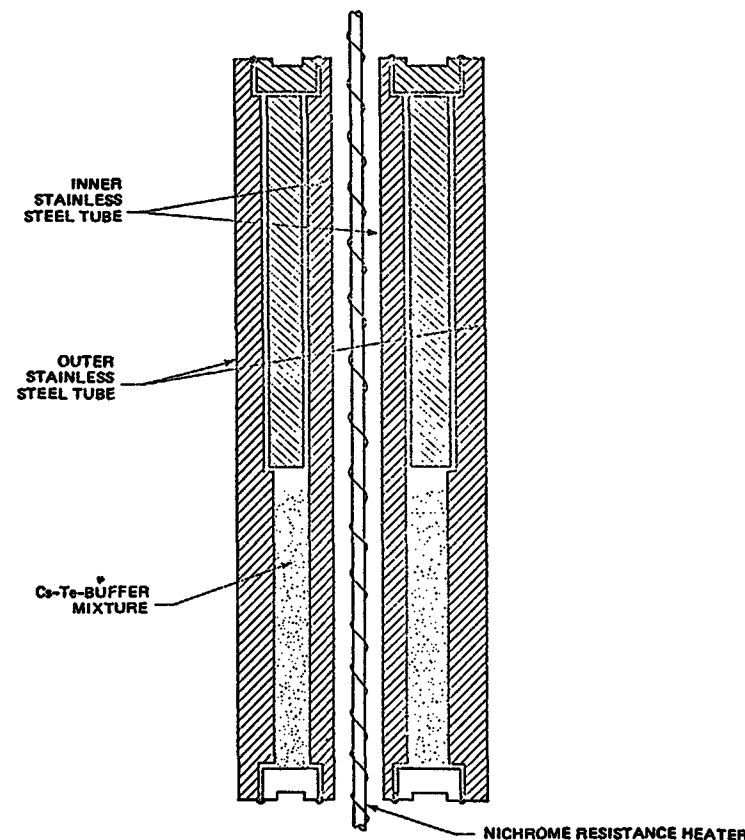

INNER STAINLESS STEEL TUBE

OUTER STAINLESS STEEL TUBE

Cs-Te-BUFFER MIXTURE

Cs-Te-BUFFER MIXTURE

NICHROME RESISTANCE HEATER

Figure 19. Annular Type-316 Stainless Steel Temperature Gradient Capsule (Not to Scale)

A. Thermodynamic Basis for Cladding Attack Inhibition (CAI)

The principal function of buffer-getter materials added to fuel pins is to act as a preferred oxygen sink, thereby reducing oxidation of the cladding. The key to successful application of a particular buffer-getter concept is simultaneous maximization of the buffer-getter oxidation rate and the rate of transport of oxygen from the fuel to the buffer-getter material.

Candidate materials can be separated into buffers and getters by considering their relative affinity for oxygen. In this context, buffers can be considered those elements which will maintain a fixed fuel O/M under given conditions but will not ordinarily reduce the fuel to an O/M below its nominal value and certainly not below an O/M of 1.875 (for $U_{0.75}Pu_{0.25}O_{2-x}$). Elements suitable for this use are vanadium, niobium, and chromium. Getters, on the other hand, may actually reduce the fuel below the O/M corresponding to its lower phase boundary, thus producing free metal. Examples of getters are zirconium, uranium, titanium, and certain rare earth metals.

The selection of candidate buffers is based on the thermodynamic stabilities of their oxides relative to that of the mixed-oxide fuel. This is most easily illustrated by means of an Ellingham plot, such as that presented in Figure 21. In general, at a fixed O/M ratio, whether it be for the fuel or a buffer oxide, equilibrium oxygen potentials increase with temperature for all the materials under consideration.

At typical fuel-cladding interface temperatures in operating pins (800-900°C) an effective buffer-getter additive must maintain the outer-surface fuel O:M at about 1.997, or lower, so that oxidation of chromium in the cladding alloy does not occur. Examination of Figure 21 reveals that the following pairs of co-existent phases all have the potential to prevent oxidation of alloyed chromium: Ti/TiO, TiO/Ti$_2$O$_3$, V/VO, Nb/NbO, NbO /Nb O$_2$(?) and Cr/Cr$_2$O$_3$. Clearly, the final choice of a buffer candidate cannot be made until other pertinent physical and chemical properties, neutronics, and oxidation kinetics have been evaluated. Experimental verification of inhibitor effectiveness is necessary because of uncertainties in some of the pertinent thermodynamic data.

B. General Efficacy of Potential Cladding Attack Inhibitors.

Some early temperature gradient experiments performed at GE [1] showed that Nb powder and Nb foil, when interspersed in and between stoichiometric fuel pellets, measurably decreased the amount of Cs,Te-induced intergranular attack in 316SS cladding positioned at the cool end of the capsules.

(a) As-Polished 40X

Hot Wall   Cooler Wall

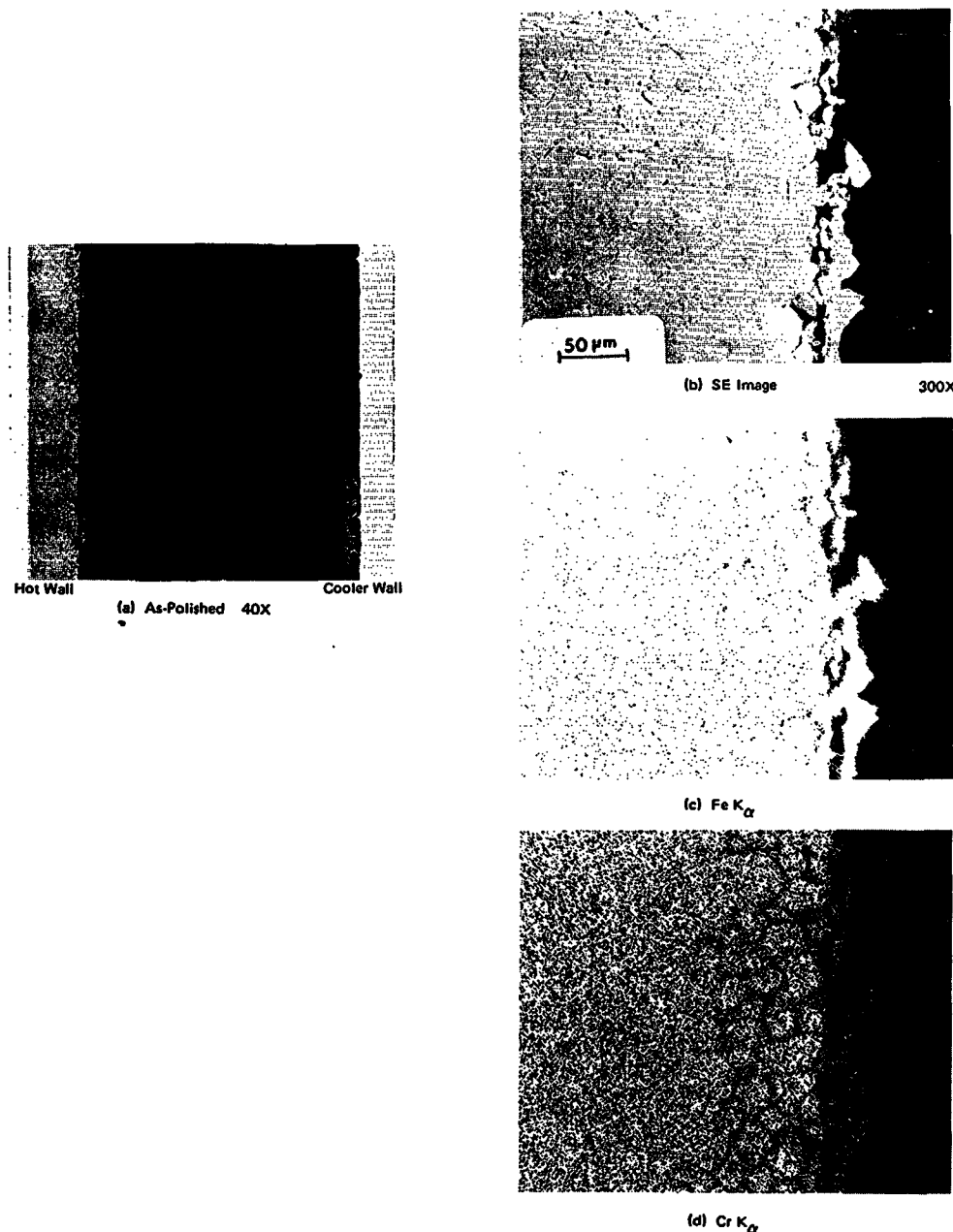(b) SE Image   300X

50 µm

(c) Fe K$_\alpha$

(d) Cr K$_\alpha$

FIGURE 20   PHOTOMICROGRAPHS AND CHARACTERISTIC X-RAY IMAGES OF TYPE-316 STAINLESS STEEL SURFACE INSIDE ANNULAR TEMPERATURE GRADIENT CAPSULE
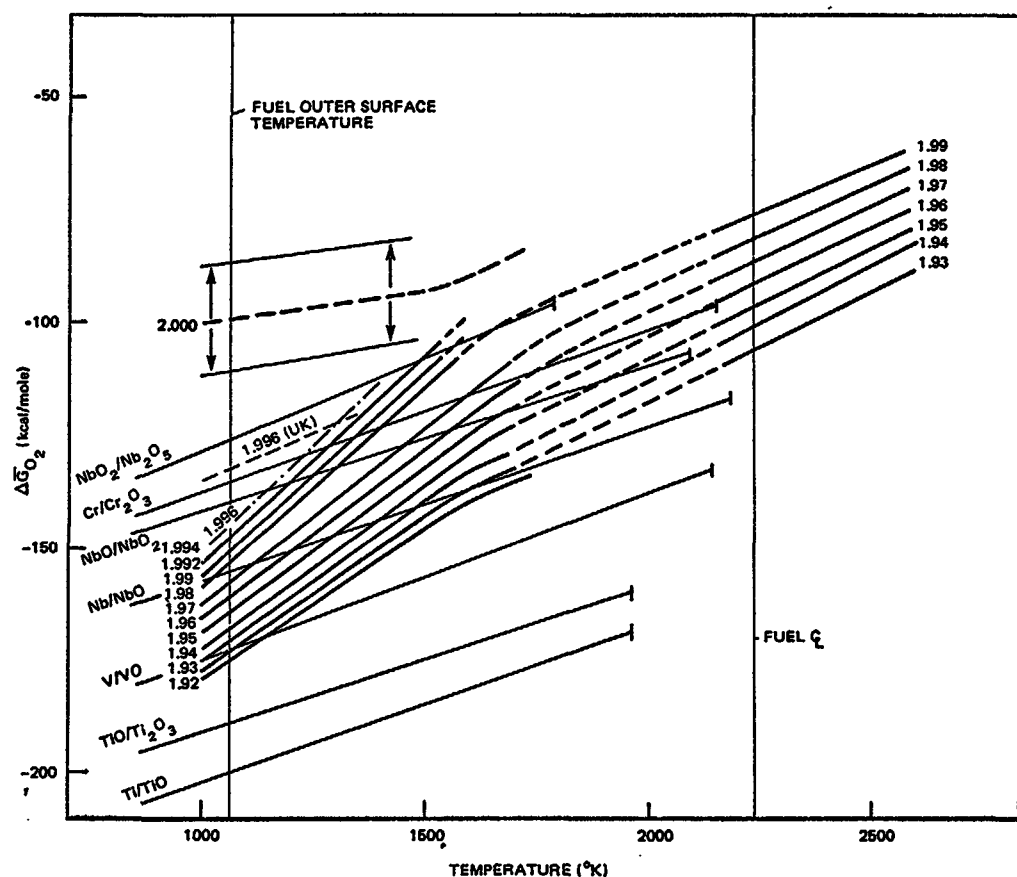
Figure 21 Oxygen Potential Diagram Showing Data for Mixed Oxide Fuel (25% Pu) and Candidate Buffers

The isothermal capsule results described in section III-B [22] demonstrated that at 725°C, Cs,Te-induced intergranular attack of 316SS did not occur at the oxygen activities established by Nb/NbO and NbO/NbO$_2$ buffer mixtures but did occur with VO/V$_2$O$_3$. According to Table 3 the oxygen potential of VO/V$_2$O$_3$ is only 5 kcal/mol greater than that of Cr/Cr$_2$O$_3$ (at 725°C). Previous isothermal capsule experiments have shown that Cr/Cr$_2$O$_3$ buffer effectively inhibits Cs,Te-induced intergranular attack of Type-316SS.[3]

Another capsule design has been used to test the efficacy of liquid NaK and Nb foil as cladding attack inhibitors. Sandwich-configuration Type-316SS specimens, of the type described in section III-F , were loaded with Cs,Te-buffer mixtures and heat treated either in the presence of liquid NaK or with a niobium

foil positioned inside the "sandwich". Both types of additive proved to be extremely effective at inhibiting deep Cs,Te-induced intergranular penetration of Type-316 stainless steel at 725°C (200 hours). In the presence of (excess) NaK, the two test specimens that were simultaneously exposed to corrosive Cs+Te mixtures did not show any signs of attack. The primary influence of the NaK is believed to be suppression of the Te activity, but reaction of the alkali metal(s) with the chromium oxide of the buffer mixture would also reduce the oxygen activity to a value below the Type-316 stainless steel oxidation threshold (analogous effect to that of sodium-fuel reaction in a breached fuel rod). In the niobium foil test a few isolated regions on the stainless steel sample surface showed a small amount of matrix reaction ($\leq$1 mil/ 25μm depth), but the remaining surface showed no signs of intergranular attack. From the metallography performed on this sample it was concluded that the attacked regions corresponded to areas where the niobium foil did not make close contact with the stainless steel. Presumably at these locations the oxygen activity remained above the oxidation threshold sufficiently long for a limited amount of attack to occur.

C. Effects of Kinetic Factors on Buffer-Getter Efficacy

Oxygen uptake by a buffer-getter system in an operating fuel pin may be less than optimum due to kinetic limitations. The results discussed in the previous section were obtained under nearly ideal conditions, i.e. with the buffer and potentially corrosive fission products in intimate contact. In certain CAI concepts the inhibitor is quite remote from the fuel-cladding interface (e.g. when it is positionned in the axial blanket), so the oxygen transport rates become important. Also, because the fuel continuously generates oxygen during irradiation, it is necessary that the inhibitor absorbs (reacts with) oxygen as fast as it is released.

Early indications of the oxidation behavior of Nb in direct contact with stoichiometric mixed oxide fuel were obtained from capsule experiments.[1] Extensive oxidation of Nb discs was observed in the temperature range 728-1100°C, whereas below 728°C only thin oxide films formed on the discs in 100 hours. Increasing the surface area of the niobium, by using pressed powder instead of discs, resulted in higher rates of oxygen uptake.

A more recent experimental study was undertaken at GE [32] to measure axial oxygen migration rates with UO$_2$ interposed between the absorber (Ti and Nb) and the fuel, and to establish the behavior of absorbers in direct contact

with fuel. Titanium and niobium were selected as absorbers because they represented two types of materials suitable for use in the LMFBR. The experimental arrangement for measuring the axial oxygen migration was similar to that used previously in oxygen and fission product thermomigration experiments.[1,3] A sealed six-inch length of Type 316 stainless steel tubing contained about 13 typical LMFBR mixed oxide pellets at the hot end and two to three UO_2 pellets interposed with a Nb powder pellet in a stainless steel cup in the manner shown in Figure 22. The sealed capsules were placed in a temperature gradient ranging from about 550°C at the cold end to 1100°C at the hot end. The capsules were positioned along the temperature gradient to achieve the desired temperature of the Nb pellet. Several different O:M ratios were used to determine the effect of oxygen activity and several heat treatment times were used. The oxygen migration rate was followed by measurement of the weight gain of the absorber, by analysis of the absorber for oxygen and by change in over-all O:M of the mixed oxide fuel. Cesium metal was added to the cold end of the capsule in some tests since previous work had shown that oxygen migration rates would be enhanced. It was found, however, that cesium tended to concentrate in the absorber, thus negating the experimenters ability to measure the oxidation rate. Some radial thermal gradient experiments were also performed using a center-heating apparatus to determine the rates of oxidation and final O:M when Nb or Ti were in direct contact with the fuel. In this arrangement a stack of annular pellets 7/8-inch in diameter were heated by a center tungsten rod. Two mixed oxide pellets were surrounded by a foil of titanium or niobium. The temperature of the foil was maintained at 1100°C for 5 hours, while the temperature of the fuel ranged from slightly above 1100°C at the periphery to near 2000°C at the center. The initial O:M of the fuel pellets was 1.968. The oxidation was measured by the final O:M, by the weight change of the fuel pellet and, where possible, by the oxygen content of the absorber.
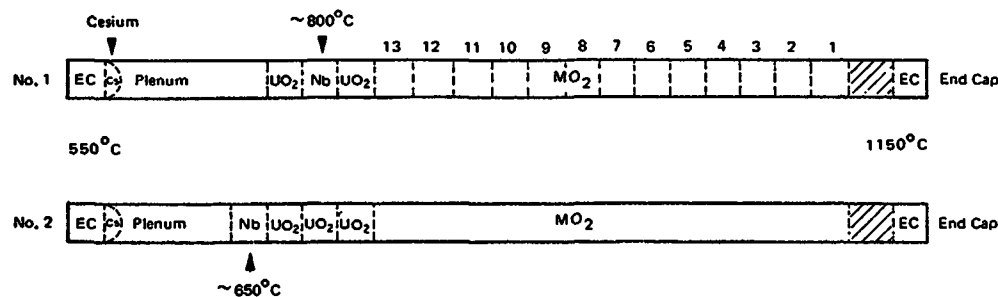

FIGURE 22 SCHEMATIC DIAGRAM OF THERMAL GRADIENT CAPSULES CONTAINING MIXED OXIDE PELLETS, UO_2 AND OXYGEN ABSORBERS

The results from these experiments are summarized in Table 7. Since a detailed discussion of these results has already been published [32], only their main features will be described here. Post-test axial distributions of Cs-137 in the capsules to which cesium was added showed a close association of the Cs to the Nb absorber and UO_2 pellet, and a general absence of Cs in the fuel. Essentially three sets of axial temperature gradient experiments were performed, with fuel O:M ratios equal to 1.965, 1.98 and 2.00. In all the test capsules that did not contain Cs the weight gains of the absorbers were very small (<2 mgm), however their measured oxygen contents were significantly higher than background levels for 1.98 fuel (at 865°C only) and 2.00 fuel (at "low" and "high" temperatures). In the 2.00 fuel capsules the oxygen contents of the absorbers were approximately one order of magnitude higher than they were with 1.98 fuel, apparently reflecting higher fuel-absorber transport rates due to the increased oxygen activity of stoichianetric fuel. Larger average O:M changes were measured for 2.00 fuel than for 1.98 fuel, however, for 2.00 fuel some of the measured ΔO:M was shown to be due to oxygen uptake by the 316SS cladding. It was concluded from the results of the axial gradient tests that the type and the temperature of the absorber were not limiting their ability to absorb oxygen. Rather, transport between the mixed oxide fuel and the absorber appeared to be the rate limiting step. From comparisons of estimated and measured oxygen fluxes in an irradiated fuel pin it was concluded that Nb or Ti absorbers would not be effective if placed in the plenum or in the blanket too far from the fuel.

Results from the radial gradient experiments showed that Ti produced the greatest O:M decrease in the fuel (ΔO:M = 0.035 for Ti, = .006 for Nb). The final fuel O:M values were believed to represent "equilibrium" values for fuel in direct contact with the absorbers at 1100°C. As expected for radial temperature gradients, the effective oxygen transport rate from the fuel to the absorber was rapid, being approximately 2 or 3 orders of magnitude higher than the corresponding axial transport rate over UO_2 at 800-900°C.

D. Chemical Interactions between Buffer/Getter Materials and Fission Products

A variety of laboratory capsule tests have been performed to evaluate the possibility of chemical interactions occurring between Cs fission products and oxidized buffer-getter products inside irradiated fuel pins [14] The tentative conclusion drawn from some early results was that Cs vapor (10^{-2} - 10^{-1} atm) reacts with Nb oxides (NbO, NbO_2, Nb_2O_5) at 800°C, with swelling, to form fairly stable complex oxides, such as $CsNbO_3$ or $CsNbO_2$.

TABLE 7 Oxygen Absorber Experiments

Experiment No.	Experiment Type	Fuel	Absorber and Wt., gm	Absorber Temperature, °C	Simulation Type	Fuel Temperature Range, °C	Fuel $\Delta T/\Delta X$ °C/cm	Time, h	Fuel Stoichiometry Change	Absorber Wt. Gain, mg	Absorber† O_2 Content, ppm	Heat of Transport kcal/mole	Oxygen Flux in Fuel micromoles/cm²/h
1*	Axial	$U_{0.75}Pu_{0.25}O_{1.965}$	Nb, 0.294	860	Blanket	1130- 952	22	100	<0.001	46.5	—	-11.5	5.1
2*			Nb, 0.338	763	Plenum	1130- 952	22	100	<0.001	36.4	6260	-11.5	3.1
3*			Ti, 0.152	754	Blanket	1102- 865	29	100	<0.001	18.8	1146	- 5.0	3.7
4*			Ti, 0.147	668	Plenum	1102- 865	29	100	<0.001	17.0	8171	- 7.6	3.9
5*			Nb, 0.272	760	Blanket	1120- 855	32	1000	<0.001	51.6		-11.2	0.4
6*			Nb, 0.301	665	Plenum	1120- 855	32	1000		53.7			
7*			Ti, 0.140	760	Blanket	1120- 855	32	1000		27.8			
8*			Ti, 0.143	665	Plenum	1120- 855	32	1000		43.2			
9*			Nb, 0.288	753	Blanket	1124- 860	32	100	<0.001	5.0	1535	- 2.1	2.9
10*			Nb, 0.290	650	Plenum	1124- 860	32	100	<0.001	24.0	9012	- 3.6	2.4
11		$U_{0.75}Pu_{0.25}O_{1.98}$	Nb, 0.288	865	Blanket	1087- 941	23	365	<0.001	2.0	320	-12.4	0.4
12			Nb, 0.296	775	Plenum	1087- 941	23	365	<0.001	0.9	90	- 6.8	0.3
13			Ti, 0.151	865	Blanket	1087- 941	23	365	NYA	2.2	870	-20.4	0.5
14			Ti, 0.141	775	Plenum	1087- 941	23	365	NYA	1.6	460	- 5.0	0.2
15a		$U_{0.75}Pu_{0.25}O_{2.00}$	Nb, 0.294	735	Blanket	1145 840	37	100	-	1.0	1870	-	-
16a			Nb, 0.302	640	Plenum	1145- 840	37		-	1.0	1930	-	-
17a			Ti, 0.149	735	Blanket	1145- 840	37		-	0.8	4060	-	-
18a			Ti, 0.149	640	Plenum	1145- 840	37		-	0.7	4170	-	-
15b			Nb, 0.298	930	Blanket	1115 990	16		0.0045	1.0	1400	~-32.0	0.6
16b			Nb, 0.297	850	Plenum	1115 990	16		--	-	NYA	-	-
17b			Ti, 0.149	930	Blanket	1115- 990	16		0.005	0.6	7730	~-32.0	0.7
18b			Ti, 0.149	850	Plenum	1115- 990	16		--	-	NYA	-	-
1R	Radial	$U_{0.75}Pu_{0.25}O_{1.968}$	Ti	1100	—	1990--1120	1054	5	-0.035	—	—	—	130.0
2R			Nb	1095	—	1950--1110	1048	5	-0.006	—	—	—	22.0

*Experiments 1 through 10 contained 25 mg Cs to aid oxygen transport; experiments 1 through 4 were carried out in N_2-6% H_2. All succeeding experiments used Ar-6% H_2 to avoid nitriding.

†Ti Blank = 400 ppm and Nb blank - 150 ppm

NYA — Not yet available

Next, two series of capsule experiments were performed to determine whether there are any differences between the reaction behavior of Nb oxides with Cs vapor and with liquid Cs. In one series, pre-measured NbO, NbO_2, and Nb_2O_5 pellets were exposed to Cs vapor at 775°C in two-temperature-zone stainless steel capsules. A pool of liquid Cs in the bottom of each capsule (360°C) established a Cs vapor of 9.7×10^{-3} atm in the vicinity of the pellets. After 100 hours all the pellets had undergone concomitant volumetric expansion ($NbO < Nb_2O_5 < NbO_2$) and weight increases ($NbO < NbO_2 < Nb_2O_5$). In a second series of tests performed in nickel capsules, Nb oxide pellets were immersed in liquid Cs during the 775°C/100 h (isothermal) heat treatments. Upon opening this set of capsules all the Nb oxide specimens were found to have undergone considerable expansion (Nb_2O_5 crumbled). Reacted pellets from both sets of capsule experiments were then heated under vacuum at various temperatures (800, 900 and 1000°C), their weight changes determined and, in some cases, their products analyzed by x-ray powder diffraction techniques. Results from these measurements showed that,after reaction with Cs at 775°C, NbO was essentially unchanged, NbO_2 was converted to NbO plus an unidentified phase, and Nb_2O_5 was almost completely converted to the same unidentifiable phase. After vacuum-distillation of a Cs-reacted Nb_2O_5 sample at 1000°C, approximately 30% by weight of Cs was retained.

Additional information about the reaction tendencies of elemental Cs with the various Nb oxides at 600-1300°C was obtained from a series of thermomigration experiments. In these experiments, small quantities of ^{137}Cs-tagged cesium metal (∼50 mgm) were initially placed at one end of 8-1/2 inch long molybdenum capsules containing columns of co-existent Nb oxide pellets (50:50 molar mixtures of $Nb+NbO$, $NbO+NbO_2$ and $NbO_2+Nb_2O_5$). The capsules were then heated in a 1300°C-600°C temperature gradient for two consecutive 100 hour periods with the ends containing the Cs additive in the hottest zone. Migration of cesium down the axial temperature gradient was followed by gamma-scanning the capsules after each 100 hour heat treatment. The results vividly demonstrated the increasing reaction tendency of Cs with Nb oxide as oxygen activity (O:Nb ratio) increases. In the Nb+NbO capsule (O:Nb=1:2), cesium had completely migrated to the cool end within 100 hour, such behavior being typical for elemental Cs. In the NbO+NbO$_2$ capsule (O:Nb=1.5:1), all the Cs had concentrated at the mid-point of the capsule after 200 hours, a position which corresponded to ca. 1050°C in the axial temperature gradient. In the $NbO_2+Nb_2O_5$ capsule (O:Nb=2.25:1), after 200 hours, Cs had scarcely moved from the hot end, being located in a sharp peak at ∼1300°C. These results confirmed the earlier (isothermal) observations that both NbO_2 and Nb_2O_5 react with

cesium, but also gave a measure of the temperature stability limits of the reaction product as a function of oxygen activity. X-ray diffraction measurements on the Cs-rich Nb oxide pellets from these capsules confirmed that the same Cs_xNbO_y product was formed as in the isothermal tests.

Some preliminary data on the thermodynamics of the Cs + Nb_2O_5 reaction when liquid Cs is in excess have been obtained from high temperature EMF cell experiments performed at GE.[31] The EMF cell design used in these studies was the same as that recently employed to characterize the sodium-fuel reaction [33]. Oxygen activity measurements were made on reacting mixtures of excess liquid cesium plus Nb_2O_5 at 650°C and these showed that the equilibrium oxygen potential is approximately -149 kcal/mol. In Figure 5 these data are compared with other EMF cell data for the Cs-U-O and Cs-O systems and also predicted $\Delta \bar{G}_{O_2}$ - T data for coexistent Nb/NbO and Cs(ℓ)/"Cs_2O"; in each case the reference electrode is co-existent In/In$_2$O$_3$. The results indicate that the reactivity of Cs fission products with Nb oxidation products is only slightly less than their reactivity with oxide fuel. This finding implies that Cs-Nb oxide chemical interaction can effectively extend the buffering capacity of a given quantity of Nb; viz. by reactions such as:

$$Cs + <NbO> + [O]_{fuel} = <CsNbO_2>$$

$$and\ 2Cs + <NbO_2> + [O]_{fuel} = <Cs_2NbO_3> .$$
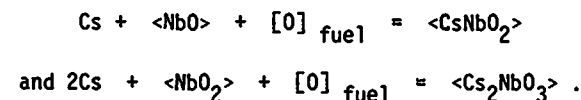
In fuel pins containing Nb as a cladding attack inhibitor cesium fission products will thus be expected to concentrate where the Nb is located.

Evidence that titanium dioxide, TiO_2, also undergoes extensive chemical interaction with cesium has been obtained from laboratory capsule experiments. TiO_2 pellets heated at 650° and 750°C in the presence of Cs vapor at unit activity underwent considerable volumetric expansion (>200%$\Delta V/V$) and retained large amounts of cesium (equivalent Cs:Ti≥1:1). The principal reaction product appears to be a Cs-Ti-O terary oxide, either $CsTiO_3$ or Cs_2TiO_3.

E. Compatibility between Buffer/Getter Materials and 316SS Cladding

Successful application of cladding attack inhibitor/oxygen absorber concepts to high performance LMFBR fuel pins requires that the candidate materials be compatible with austenitic stainless steel cladding for extended periods at the applicable cladding inner surface temperatures (600-760°C). Several

series of laboratory capsule annealing experiments were conducted at HEDL to evaluate possible compatibility problems between 316SS cladding and Ti, V and Nb prior to in-reactor testing.[27b] Four different capsule configurations were used in this study which was performed at 700 and 800°C. Two of the capsule designs employed the split cladding halves concept that was used for some FCCI tests (see Figure7c). In this design, in which Ti- and V-coated fuel pellets and porous Ti pellets were tested, contact pressure between samples and the cladding was due only to the pellet weight. An upright capsule design was used to obtain data for Ti - 316SS planar contact interfaces with contact pressure determined by the weight of the stainless steel pellets. Similar capsules with threaded end bolts that could be torqued to 20 ft-lbs were used for preliminary high contact pressure tests with Nb, V and Ti powders and foils. These various capsule designs are illustrated in Figure 23.

The initial pressure-contact experiments indicated the existence of potential compatibility problems between Ti and V metals and 316 stainless steel at 800°C,

the stainless steel surfaces being affected to depths up to 13 microns (1/2 mil) after 137 hours. No reaction between niobium and 316SS was observed under these conditions. In atmospheres with low oxygen content, low-pressure contact between Ti and 316SS produced 30 micron depth reaction zones at 800°C (568 hours), but no reaction at 700°C. In the presence of oxide fuel (O:M=1.98), neither Ti or V reacted with 316SS at 800°C. This difference in behavior due to the presence of oxide fuel was attributed to the fuel's ability to maintain a passive oxide layer at cladding-absorber interfaces (i.e. an oxygen inventory effect). Based on the low oxygen activity Ti penetration data at 800°C it was estimated that 639 days would be required to cause 75μ/3 mils of cladding inner surface reaction under the worst possible conditions. Since cladding inner surface temperatures in irradiated fuel pins are unlikely to exceed 750°C, and since absorber surfaces would be partially oxidized and/or reacted with fission products, it was concluded that incompatibility between Nb, Ti or V and 316SS cladding is unlikely to be a problem.
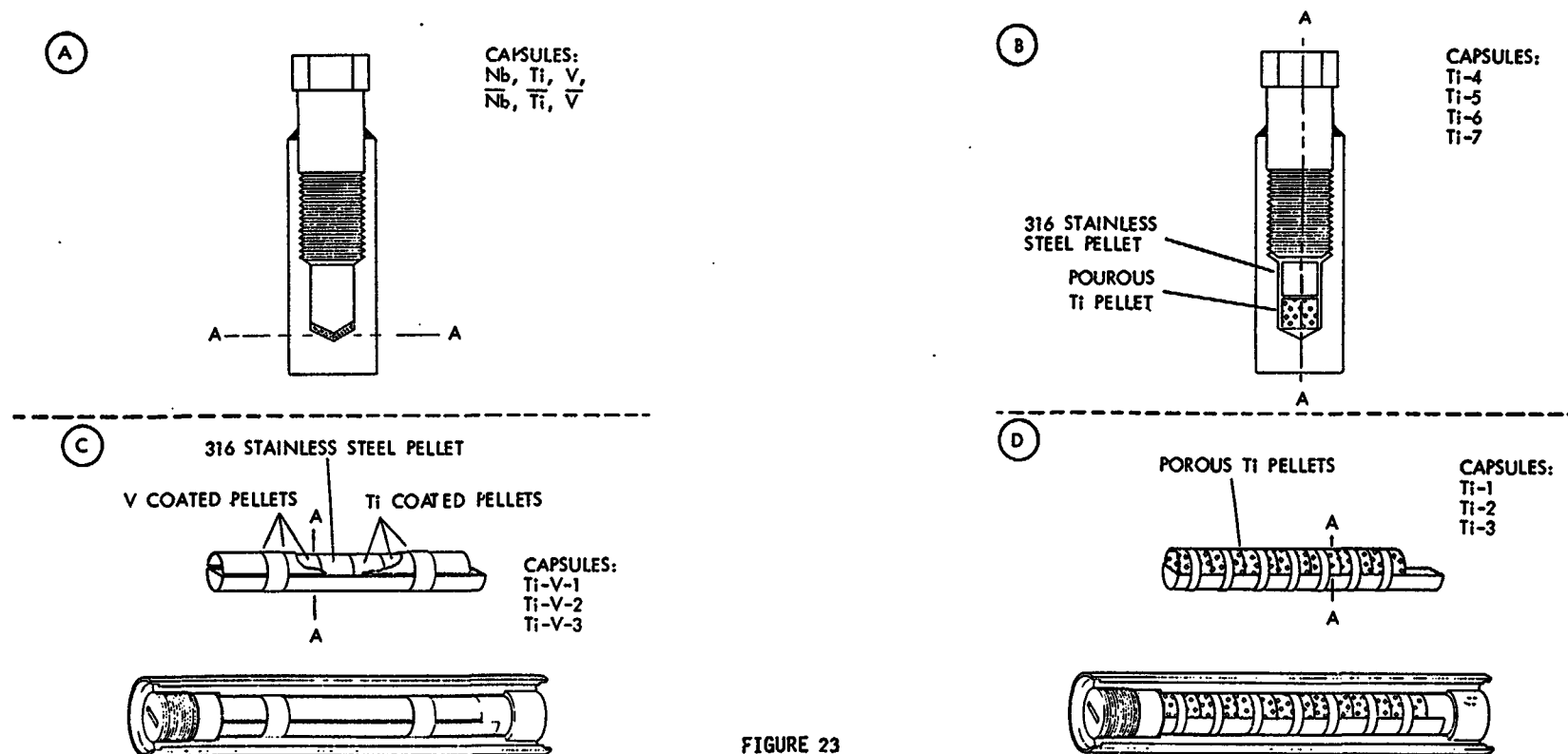

FIGURE 23

Capsule Designs for Cladding-Absorber Compatibility Tests.

REFERENCES

1. E.A. Aitken , S.K. Evans, B.F. Rubin, and T.E. Ludlow, "Transport and Reaction of Cs, Te, I and Mo with Fast Reactor Fuel and Stainless Steel Cladding: I, "GE-FBRD, GEAP$\approx$12268 (November 1972); see also "Behavior and Chemical State of Irradiated Ceramic Fuels", IAEA, Vienna, 1974, p. 269.

2. C.E. Johnson, I. Johnson, P. Blackburn, J.E. Battles, and C.E. Crouthamel, "Behavior and Chemical State of Irradiated Ceramic Fuels", IAEA, Vienna, 1974, p.1.

3. E.A. Aitken, M.G. Adamson, D. Dutina, and S.K. Evans, "Thermomigration and Reactions of Fission Products in Breeder Reactor Oxide Fuels: II. Out-of-Pile Investigation of Cs- and Te-Induced Attack of Type-316 Stainless Steel Cladding", GE-FBRD, GEAP-12538 (Sept. 1974); see also "Thermodynamics of Nuclear Materials 1974, Vol. 1," IAEA, Vienna, 1975, p. 187.

4. M.G. Adamson, "Mechanisms of Fuel Cladding Chemical Interaction: US Interpretation", this meeting.

5. P.E. Blackburn, in ANL-75-48 (March 1976).

6. R.E. Woodley, private communication.

7. R.E. Woodley, Journal of American Ceramic Society, 56 (1973) p. 116.

8. M. Tetenbaum, "Thermodynamics of Nuclear Materials 1974,Vol. II", IAEA, Vienna, 1975, p. 305; also Transactions ANS, 23 (1976), p. 131.

9. T.L. Markin and E.J. McIver, "Putonium 1965", ed. A.E. Kay and M.E. Waldron on (1967), p. 845.

10. T.L. Markin and M.H. Rand, "Thermodynamics of Nuclear Materials 1967", IAEA, Vienna (1968), p. 637.

11. T.L. Markin and E.C. Crouch, Journal of Inorganic Nuclear Chemistry, 32 (1970), p. 77.

12. P.A.G. O'Hare, et al., "Thermodynamics of Nuclear Materials 1974, Vol. II" IAEA, Vienna, 1975, p. 439.

13. P.A.G. O'Hare, et al., Journal Chem. Thermodynamics, 8 (1976) p. 845; 8 (1976) p. 381; 8 (1976) p. 353; 8 (1976) p. 255, 7 (1975) p. 831.

14. I. Johnson, Journal Physical Chemistry 79 (1975), p. 722.

15. E.H.P. Cordefunke, "Thermodynamics of Nuclear Materials 1974, Vol. II" IAEA, Vienna, 1975, p. 185.

16. I. Johnson, in ANL-75-48 (March 1976).

17. S.K. Evans and E.A. Aitken, "Oxygen Redistribution in (U,Pu) O_{2-x} Fuels" GEAP-14036 (January 1975).

18. P.E. Blackburn and C.E. Johnson, "Thermodynamics of Nuclear Materials 1975, Vol. I", IAEA, Vienna (1975) p. 17.

19. M.G. Adamson, et al., "Thermodynamics of Nuclear Materials 1974, Vol. I", IAEA, Vienna (1975) p. 17.

20. G. Romeo and D.W. McKee, J. Electrochem. Soc. 122, No. 2 (1975) p. 188.

21. H.E. McCoy, Molten Salt Reactor Program Semi-Annual Report ORNL-4832 (September 1972), p.64.

22. M.G. Adamson and E.A. Aitken, "Recent Advances in the Mechanism of Fission-Product-Induced Intergranular Attack in Type 316 Stainless Steel Cladding" GEAP-14136 (August 1976).

23. P.S. Maiya and D.E. Busch, Metallurgical Transactions A, 6A, (1975) p. 409.

24. M.G. Adamson, E.A. Aitken, S.K. Evans, and W.H. McCarthy, "Prediction of Fuel-Cladding Chemical Interaction in Irradiated Mixed-Oxide Fuel Rods", GE-FBRD, GEAP-14075 (December 1976).

25. M. Kangilaski and M.G. Adamson, "Chemical Attack of Prospective Advanced Cladding Alloys in Simulated Mixed Oxide Fission Product Environments", GE-FBRD, to be issued at a later date.

26. D.W. McKee, D. Chatterji, and G. Romeo, Corrosion Science 16, No. 4, 1976, p. 253.

27. C.N. Wilson, (a) "Effects of Al, Ca, and Si Fuel Impurities on Fuel-Cladding Compatibilty", HEDL TME 76-30 (April 1976): (b) "Compatibility of Niobium, Titanium and Vanadium Metals with LMFBR Cladding", HEDL TME 75-100 (October 1975).

28. O. Gotzmann, P. Hoffmann, and F. Thummler, J. Nucl. Mat., 52 (1974) p. 33.

29. D.C. Fee, I. Johnson, and C.E. Johnson, "Chemical Interaction Between Fuel and Cladding in Stainless Steel-Clad Fast Reactor Fuels", Argonne National Laboratory Report, ANL-75-53 (October 1975).

30. I. Johnson and C.E. Johnson, "Thermodynamics of Nuclear Materials 1974, Vol. I" IAEA, Vienna (1975) p. 99.

31. M.G. Adamson, "Transport and Reactions of Cesium Fission Products in Oxide Fuel Rods", American Ceramic Soc. Bulletin 55 (September 1976). p. 819.

32. E.A. Aitken et al., A Thermodynamic Data Program Involving Plutonia and Urania at High Temperatures, Quarterly Report No. 22, November 1, 1972 - January 31, 1973, GE-FBRD, GEAP-12466 (December 1972).

33. M.G. Adamson, "Sodium-Fuel Reaction Studies: Fuel Pellet Swelling Behavior and Alkali Metal-Oxide Fuel Reaction Thermodynamics, GE-FBRD, GEAP-14093 (March 1976),